The Astrophysical Journal, 631:000–000, 2005 October 1

MAGNETIC FIELD CONFINEMENT IN THE SOLAR CORONA. II. FIELD-PLASMA INTERACTION

N. Flyer,[1] B. Fornberg,[2] S. Thomas,[1] and B. C. Low[3]
Received 2005 May 2; accepted 2005 June 11

ABSTRACT

Q1 The numerical study of axisymmetric force-free magnetic fields in the unbounded space outside a unit sphere, presented in the first paper of this series, is extended to treat twisted fields in static equilibrium with plasma pressure and weight in a polytropic atmosphere. The study considers dipolar magnetic fields all sharing the same boundary flux distribution on the unit sphere and characterized with (1) a nonlinear distribution of its azimuthal field component expressed as a power of the poloidal flux function and (2) a plasma distribution varying linearly with the poloidal flux function. Nonlinear boundary value problems are solved numerically to generate a continuum of solutions with two parameters to control the total azimuthal flux and the strength of field-plasma interaction. The study includes the force-free fields of the first paper as a special case. Models with polytropic indices $\Gamma = 7/6$, $14/11$ are treated to show the interplay between the degree of magnetic twist and hydrostatic stratification in determining atmospheric structures, with particular interests in magnetic flux ropes and their storage of magnetic energy and azimuthal flux at levels above those bounds applicable to force-free fields. The concluding discussion relates physical insights from the study to the solar corona and the energetics of coronal mass ejections and flares.

Subject headings: MHD — Sun: corona — Sun: coronal mass ejections (CMEs) — Sun: prominences

1. INTRODUCTION

In the first paper of this series, we treated the self-confinement of nonlinear force-free magnetic fields in axisymmetry outside a unit sphere representing a theoretical star (Flyer et al. 2004, hereafter Paper I[4]). Of special interest to the study was the confinement of an azimuthal rope of twisted field by an external field anchored rigidly to the sphere under the flux-freezing condition of perfect electrical conductivity. A numerical nonlinear elliptic solver, especially developed for the study, produced several parametric families of force-free fields that demonstrated two main results. First, the flux rope can store magnetic energy in moderate excess, of the order of a few percent, of the threshold set by Aly (1984, 1991) for a spontaneous opening up of the global field, corroborating recent results (Hu et al. 2003; Wolfson 1993, 2003). Secondly, subject to a fixed amount of the poloidal flux anchored to the unit sphere, the confinement of the flux rope against its outward expansion sets a limit to the total azimuthal flux in the theoretical atmosphere. These properties are relevant to mechanisms of solar coronal mass ejections (CMEs) attributed to the failure of the confinement of a magnetic flux rope in the solar corona (see, e.g., Amari et al. 2003a, 2003b; Fan & Gibson 2003, 2004; Fan & Low 2003). Reviews of CME phenomenology can be found in Aschwanden (2004), Hundhausen (1999), Howard et al. (1985, 1997), Klimchuk (2001), Low (2001), and Zhang & Low (2005).

These results on force-free magnetic fields are expected to be modified for fields stressed by the pressure and weight of the atmospheric plasma, as pointed out in Paper I. Plasma pressure and weight play opposite roles in the mechanics of flux-rope confinement. Plasma weight can serve as an anchor to hold a flux rope to the base of the atmosphere. In contrast, pressure is not a confinement agent because it enhances the magnetic pressure to drive an outward expansion. A low-temperature plasma introduces weight with a small or negligible pressure effect and, by this consideration, may be an effective way of holding in equilibrium magnetic flux systems not directly anchored to the atmospheric base. This is probably the magnetic role of quiescent prominences in coronal structures (Tandberg-Hanssen 1995; Low & Hundhausen 1995; Low 1996, 2001; Fong et al. 2002; Low et al. 2003; Lionello et al. 2002; Zhang & Low 2004; Low & Zhang 2004; Hu & Wang 2005). Introducing a hot plasma into the equilibrium field presents an interesting but more complicated question of how gravity and pressure may play opposing roles to aid the confinement of a flux rope. This is the question we address in the present paper, by extending the force-free field model of Paper I to include these plasma effects. The extended model is treated with a modified version of our numerical elliptic solver used for Paper I.

It is an idealization to take the atmosphere of a star to be static. An atmosphere with solar coronal temperatures will always dominate over the field in its outer part to expand into a stellar wind (Parker 1963). We are suppressing the solar wind phenomenon in our model in order to address questions relating to conditions of static equilibrium at the base of the corona. Despite their relative physical simplicity, magnetic fields in static equilibrium present formidable nonlinear mathematical problems. The force-free states of a twisted magnetic field in the unbounded, axisymmetric atmosphere had defied systematic mathematical study until Paper I. The investigation reported here takes this development a step further to establish a number of elementary results regarding the influence of field-plasma interaction on the storage of energy and azimuthal flux in twisted fields.

In §§ 2, 3, and 4 we derive the governing equations, introduce the polytropic static atmosphere, and present our numerical study of equilibrium magnetic fields. Our study concentrates on basic

[1] National Center for Atmospheric Research, Division of Scientific Computing, 1850 Table Mesa Drive, P.O. Box 3000, Boulder, CO 80307; flyer@ucar.edu, thomas@ucar.edu.

[2] Department of Applied Mathematics, University of Colorado, 526 UCB, Boulder, CO 80309; fornberg@colorado.edu.

[3] National Center for Atmospheric Research, High Altitude Observatory, P.O. Box 3000, Boulder, CO 80307; low@ucar.edu.

[4] Note the following errata for Paper I: (1) on page 1214 the sign of $\partial^2 A/\partial\eta^2$ should be positive, and (2) the quantity graphed in Fig. 1 of Paper I is $\gamma e^{2s} A^5$, the nonlinear term in eq. (A1), not A.

physical properties in a highly idealized system. With these properties understood, we relate them to real solar coronal structures and phenomenology in a concluding discussion in § 5.

2. THE MAGNETOSTATIC EQUATIONS

Consider the axisymmetric, solenoidal magnetic field

$$\boldsymbol{B} = \frac{1}{r \sin\theta}\left(\frac{1}{r}\frac{\partial A}{\partial \theta}\hat{\boldsymbol{r}} - \frac{\partial A}{\partial r}\hat{\boldsymbol{\theta}} + Q\hat{\boldsymbol{\varphi}}\right), \tag{1}$$

in terms of its flux function A and the function Q describing the azimuthal field component. Substituting into the equation for force balance

$$\frac{1}{4\pi}(\nabla \times \boldsymbol{B}) \times \boldsymbol{B} - \nabla p - \frac{\rho G M_\odot}{r^2}\hat{\boldsymbol{r}} = 0, \tag{2}$$

we obtain the two governing equations

$$\frac{\partial^2 A}{\partial r^2} + \frac{1-\mu^2}{r^2}\frac{\partial^2 A}{\partial \mu^2} + Q\frac{dQ}{dA} + 4\pi r^2\left(1-\mu^2\right)\frac{\partial p(A,\ r)}{\partial A} = 0, \tag{3}$$

$$\frac{\partial p(A,\ r)}{\partial r} + \frac{\rho G M_\odot}{r^2} = 0, \tag{4}$$

with $\mu = \cos\theta$, where we have imposed the condition $Q(r,\ \theta) = Q(A)$ to satisfy force balance in the φ-direction (Hundhausen et al. 1981; Uchida & Low 1981).

We adopt the power-law form of Q introduced in Paper I:

$$Q = \sqrt{\frac{2\gamma}{1+n}}A^{(1+n)/2}, \tag{5}$$

where n and γ are constants to be freely prescribed. An equation of state or steady energy transport is required to close the system of equations for the unknowns p, ρ, and A. We adopt the polytropic model as a convenient closure and concentrate on magnetic structures.

2.1. *The Polytropic Atmosphere*

Since the Lorentz force acts perpendicular to $\boldsymbol{B}$, the static atmosphere described by equation (2) must support its weight along each field line by the pressure gradient force. The global atmosphere is thus composed of hydrostatic elements in individual magnetic flux tubes stacked, side by side, in equilibrium by the Lorentz force. Equation (4) is the hydrostatic relationship of each atmospheric element along a magnetic line of force of constant A. Let us introduce the polytropic equation of state with polytropic index Γ:

$$p = c^2(A)\rho^\Gamma, \tag{6}$$

where $c(A)$ is just a constant on each line of force parameterizing the amount of mass loaded on the field. Equation (4) can then be integrated once with respect to r to give

$$p = P(A)\left[\frac{r_0}{r_1(A)} + \frac{r_0}{r}\right]^{N+1},$$

$$\rho = P(A)(N+1)\left(\frac{GM_\odot}{r_0}\right)^{-1}\left[\frac{r_0}{r_1(A)} + \frac{r_0}{r}\right]^N,$$

$$P(A) = c^2(A)\left[\frac{1}{c^2(A)(1+N)}\frac{GM_\odot}{r_0}\right]^{N+1}, \tag{7}$$

where r_0 is a normalization length scale and $r_1(A)$ is an integration constant allowed to vary from one field line to another. We have replaced the symbol for the polytropic index with $\Gamma = 1 + 1/N$ for convenience of notation and refer to N as the polytropic power index. The problem reduces to the one for a spherically symmetric, polytropic, hydrostatic atmosphere if we take c and r_1 independent of A (Parker 1963).

On each line of force of constant A, there are two free parameters defining the polytropic atmospheric element on it: $P(A)$ fixing the amount of mass in the element, and $r_1(A)$ taken to define the temperature T_0 at some reference sphere $r = r_0$ by the ideal gas law,

$$T_0 = \frac{GM_\odot}{r_0}\frac{1}{(N+1)R_0}\left(\frac{r_0}{r_1} + 1\right), \tag{8}$$

where R_0 is the gas constant. We may identify r_0 to be the radius of a theoretical star. Negative values of r_1 are admitted for base temperatures T_0 lower than the critical value of $T_{\rm crit} = (GM_\odot/r_0)[1/(N+1)R_0]$. In such cases, provided $|r_1| > r_0$, the atmosphere extends to a finite radial distance $r = |r_1|$ where p and ρ vanish, compatible with vacuum located in $r > |r_1|$. This outer boundary of the atmosphere is, in general, not spherical in shape through the dependence of r_1 on A. An analytical solution describing such an atmosphere abutting vacuum at its top, with its magnetic field extending into vacuum, is given in the Appendix.

Positive values of r_1 are obtained for hot atmospheric elements with $T_0 > T_{\rm crit}$ that extend radially as far out as the top of the line of force of a constant A without encountering zeros in p and ρ. Moreover, if a line of force should extend to great radial distances, p and ρ would be asymptotically uniform in $r \gg r_1$. This property is related to the inverse-square falloff of Newtonian gravity in which a fixed amount of mass requires a milder pressure gradient to support its weight the farther out radially the mass is located. For near-vacuum conditions far from a theoretical star, such a uniform far pressure cannot be balanced in the far reaches. The static mathematical solution is then physically not admissible and must be replaced with a solution describing a stellar wind of the Parker (1963) theory.

The problems of hydromagnetic stellar winds are notoriously intractable (Heinemann & Olbert 1978; Sakurai 1985). The free boundary problems of static atmospheres with $T_0 < T_{\rm crit}$, illustrated in the Appendix, are also generally intractable. The marginal case of $|r_1| \to \infty$ contains an unbounded static atmosphere with vanishing pressure and density at infinity. This special case is the one we select for study in this paper (Low & Smith 1993; Wolfson & Dlamini 1997). With $r_1 \to \infty$, we have

$$p = P(A)\left(\frac{r_0}{r}\right)^{N+1}, \tag{9}$$

$$\rho = P(A)(N+1)\left(\frac{GM_\odot}{r_0}\right)^{-1}\left(\frac{r_0}{r}\right)^N, \tag{10}$$

and the field equation (3) poses the elliptic equation for A:

$$\frac{\partial^2 A}{\partial r^2} + \frac{1-\mu^2}{r^2}\frac{\partial^2 A}{\partial \mu^2} + \gamma A^n + \frac{(1-\mu^2)}{r^{N-1}}\frac{dP}{dA} = 0, \tag{11}$$

subject to suitable boundary conditions. Through the solution A, equations (1) and (7) translate $\boldsymbol{B}$, p, and ρ into explicit functions of space in a state of equilibrium.

2.2. *A Simple Model*

The dipole potential field in the space external to a unit sphere of radius r_0, defined as

$$\boldsymbol{B} = B_0\left(\frac{2r_0^3\cos\theta}{r^3}\hat{\boldsymbol{r}} + \frac{r_0^3\sin\theta}{r^3}\hat{\boldsymbol{\theta}}\right), \tag{12}$$

is generated by the flux function

$$A_{\text{potential}} = B_0 r_0^3\frac{\sin^2\theta}{r}. \tag{13}$$

We are interested in nonpotential equilibrium states for a magnetic field in $r > r_0$ having the same boundary flux as this potential field at $r = r_0$. This field satisfies the boundary conditions

$$\begin{aligned} r &= 1, \quad A = \sin^2\theta, \\ r &\to \infty, \quad |\nabla A| \to 0, \\ \theta &= 0,\ \pi, \quad A = 0. \end{aligned} \tag{14}$$

Here and elsewhere, unless otherwise stated, we carry out computations in physical units such that $B_0 = 1$ and $r_0 = 1$.

Among the rich variety of models associated with the different forms of $P(A)$ in equation (9), we select the linear distribution $P = (1/8\pi)(\beta_0 + \gamma_1 A)$, where β_0 and γ_1 are constants, for numerical investigation:

$$p = \frac{1}{8\pi}\frac{\beta_0 + 2\gamma_1 A}{r^{N+1}}, \tag{15}$$

$$\rho = (GM_\odot)^{-1}\frac{N+1}{8\pi}\frac{\beta_0 + 2\gamma_1 A}{r^N}. \tag{16}$$

This simple model is useful for a first systematic study of nonlinear magnetostatic equilibria of this type. The field is governed by

$$\frac{\partial^2 A}{\partial r^2} + \frac{1-\mu^2}{r^2}\frac{\partial^2 A}{\partial\mu^2} + \gamma A^n + \gamma_1\frac{(1-\mu^2)}{r^{N-1}} = 0, \tag{17}$$

to be solved for A in $r > 1$ subject to the boundary conditions given by equation (14).

The current density by Ampere's law is proportional to

$$\nabla\times\boldsymbol{B} = \frac{1}{r\sin\theta}\left[\frac{1}{r}\frac{\partial Q}{\partial\theta}\hat{\boldsymbol{r}} - \frac{\partial Q}{\partial r}\hat{\boldsymbol{\theta}} - \left(\frac{\partial^2 A}{\partial r^2} + \frac{1-\mu^2}{r^2}\frac{\partial^2 A}{\partial\mu^2}\right)\hat{\boldsymbol{\varphi}}\right]. \tag{18}$$

Field equation (17) therefore describes the distribution of the equilibrium azimuthal current density as the sum of two components. One component is due to a field-aligned current density, parameterized by the constant γ, that produces no Lorentz force but gives the field a twisted topology. The other component, parameterized by the constant γ_1, produces a Lorentz force kept in balance with the hydrostatic forces of the plasma. If $\gamma_1 = 0$, we regain the force-free fields of Paper I. In § 2.3 we examine the $\gamma = 0$, $\gamma_1 \neq 0$ equilibrium fields that are purely poloidal with $B_\varphi = 0$.

2.3. *The* $\gamma = 0$ *Untwisted Magnetic Fields*

Set $\gamma = 0$ in field equation (17) to obtain

$$\frac{\partial^2 A}{\partial r^2} + \frac{1-\mu^2}{r^2}\frac{\partial^2 A}{\partial\mu^2} + \frac{\gamma_1(1-\mu^2)}{r^{N-1}} = 0, \tag{19}$$

with the solution

$$A_{\gamma=0} = \left[\frac{1}{r} + \frac{\gamma_1}{(N-1)(N-4)}\left(\frac{1}{r} - \frac{1}{r^{N-3}}\right)\right]\sin^2\theta, \tag{20}$$

satisfying the boundary conditions given by equation (14) (Hundhausen et al. 1981; Uchida & Low 1981; Low & Smith 1993). Our numerical study is centered on sequences of solutions to the nonlinear field equation (17), subject to the boundary conditions given by equation (14), for an increasing γ but a fixed γ_1, starting with a $\gamma = 0$ solution given by equation (20). This solution assumes $(N-1)(N-4) \neq 0$, which is sufficient for our study. If $N = 1$ or 4, separate calculations are needed to obtain the proper solutions. We limit our attention to $N > 3$, which ensures that all $\gamma = 0$ magnetic fields have a finite total magnetic energy in $r > 1$.

The physical properties are distinct in the two regimes $3 < N < 4$ and $N > 4$. By equation (8), the base temperature T_0 is inversely proportional to $N + 1$. At lower base temperatures with $N > 4$, the pressure extending to great radial distances is negligible so that the far field is approximately potential. At higher base temperatures with $3 < N < 4$, the far pressure is significant and it stretches out the far field into a nonpotential state. We select two representative polytropes from these two regimes for the study: $N = 11/3$ and 6. A selection of the $\gamma = 0$ equilibrium fields from these two regimes is displayed in Figures 1 and 2 to show their parametric dependence on γ_1.

Consider first the $N = 6$ solutions for positive γ_1. The poloidal field is a dipole potential field for $\gamma_1 = 0$. This field is increasingly stretched outward, as γ_1 increases from 0, to trap a plasma enhancement, given by equation (15), in the equatorial region. At a critical value given by

$$\gamma_{1,\text{crit}} = N - 1, \tag{21}$$

the field changes parametrically from a purely anchored field in $r > 1$ to an anchored field trapping a bubble of completely closed field lines centered around a local maximum of A. In the case of $N = 6$, $\gamma_{1,\text{crit}} = 5$, Figures 1*b* and 2*b* show the field and plasma configuration for $\gamma_1 = 5$ where an O-type magnetic neutral point has appeared parametrically at $r = 1$, $\theta = \pi/2$. For $\gamma_1 > 5$, this O-type neutral point moves parametrically into $r > 1$ around which closed poloidal magnetic field lines circulate such as seen in the $\gamma_1 = 10$ solution shown in Figures 1*c* and 2*c*. The magnetic bubble is held in equilibrium in part by the weight of the plasma enhancement contained in it.

Since this poloidal field has an O-type magnetic neutral point where there is plasma enhancement, the ratio of the plasma to magnetic pressure is naturally extremely large near this neutral point. An unorthodox ratio β_G defined by Hundhausen et al. (1981) may be used to better characterize the plasma-field interaction on a global scale, namely, the ratio of the plasma pressure along the equator to the magnetic pressure along the polar axis at the same radial distance. As these authors explain, this parameter indicates the degree of confinement of the equatorial plasma by the high-latitude fields ($\beta_G < 1$) or the poleward compression of the latter by the equatorial plasma ($\beta_G > 1$). For the solution in Figures 1*b* and 2*b*, β_G is radially monotonically decreasing from a peak value of 2.5 at $r = 1$ to less than unity at about $r = 1.5$. If we set $\gamma_1 = 1.0$, β_G decreases from 0.5 at $r = 1$ to about 0.2 at $r = 1.5$.

For negative values of γ_1, the field in the $N > 4$ polytropic atmosphere is compressed toward the boundary $r = 1$; see the

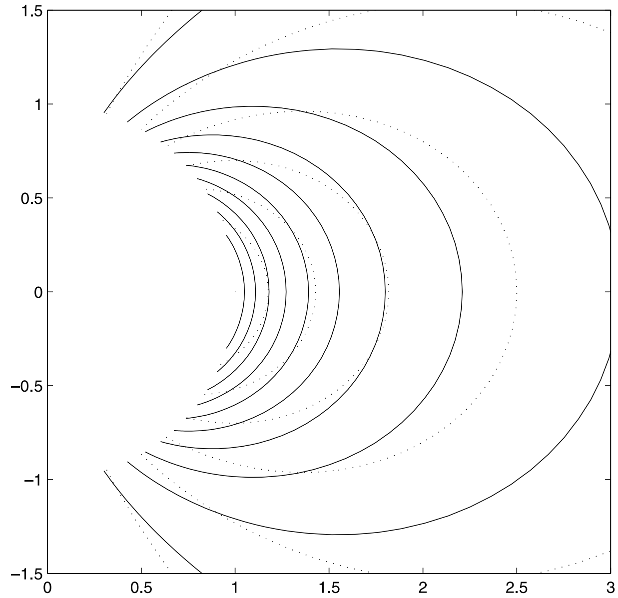

FIG. 1*a*

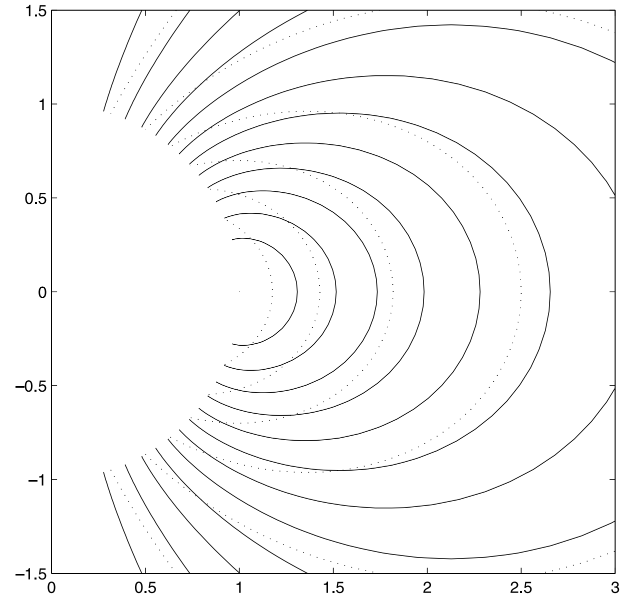

FIG. 1*b*

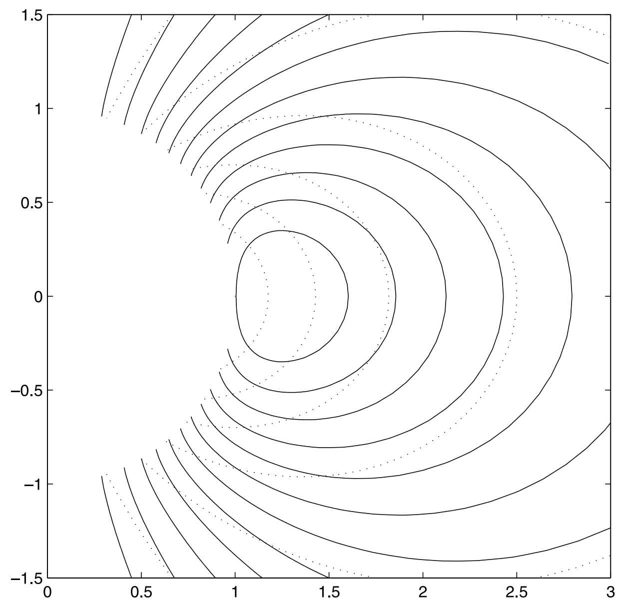

FIG. 1*c*

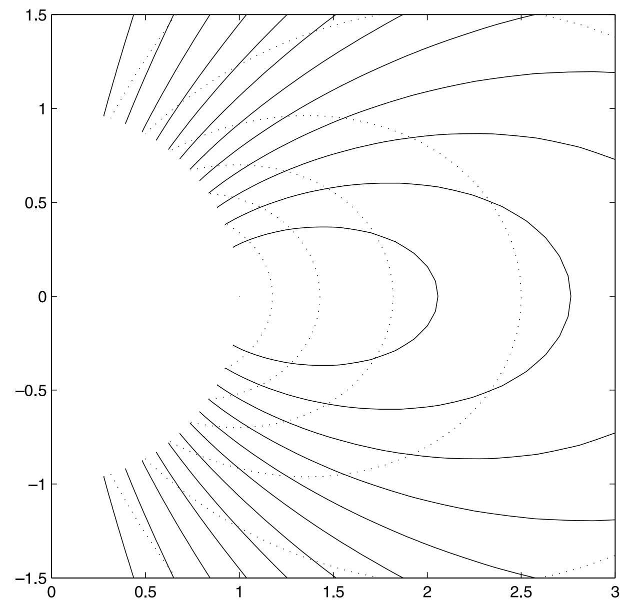

FIG. 1*d*

FIG. 1.—Poloidal magnetic lines of force (*solid lines*) of constant A on the r-θ plane in $r > 1$, superimposed with the lines of force of the potential dipole field (*dotted lines*) sharing the same normal flux distribution at $r = 1$. Both sets of lines carry the same values of A at a constant interval so that they share the same footpoints on $r = 1$. (*a*) $N = 6$, $\gamma_1 = -5$; (*b*) $N = 6$, $\gamma_1 = 5$; (*c*) $N = 6$, $\gamma_1 = 10$; (*d*) $N = 11/3$, $\gamma_1 = 3$.

example in Figures 1*a* and 2*a* for $\gamma_1 = -5$. For those solutions meeting the condition

$$|\gamma_1| < |(N-1)(N-4)|, \tag{22}$$

A is positive definite in $r > 1$. Then, for a fixed value of $\beta_0 > 0$ sufficiently large to ensure positive definite p and ρ, a negative γ_1 describes a plasma depletion centered around the equator at the base of the atmosphere. The radially inward compression of the equilibrium field at the base of the atmosphere produces a radially outward Lorentz force that partially supports the weight of the undepleted upper atmosphere. For negative values of γ_1 violating the condition given by equation (22), a line representing $A = 0$ would appear at some large r, marking a flux surface separating the main atmosphere from a second atmosphere in which $A < 0$, located above the line $A = 0$. A new magnetic bubble appears in this second atmosphere trapping a density enhancement relative to the background atmosphere. We have no interest in this regime of the γ_1 parametric space and have omitted presenting an example in Figure 1.

The global pressure ratio β_G for the solution in Figures 1*a* and 2*a* starts from a small value at $r = 1$, depending on the value of the free amplitude β_0 adopted for the background atmosphere. It then increases with r to a maximum located at a moderate radial distance before it decreases to 0 at large r. For this solution,

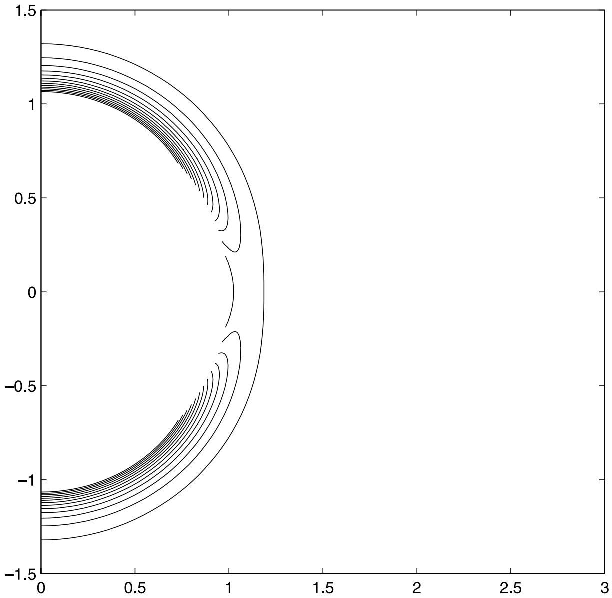

FIG. 2*a*

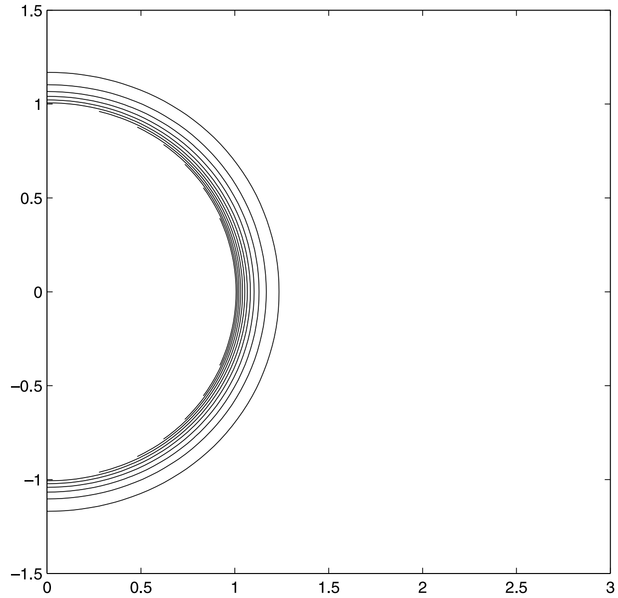

FIG. 2*b*

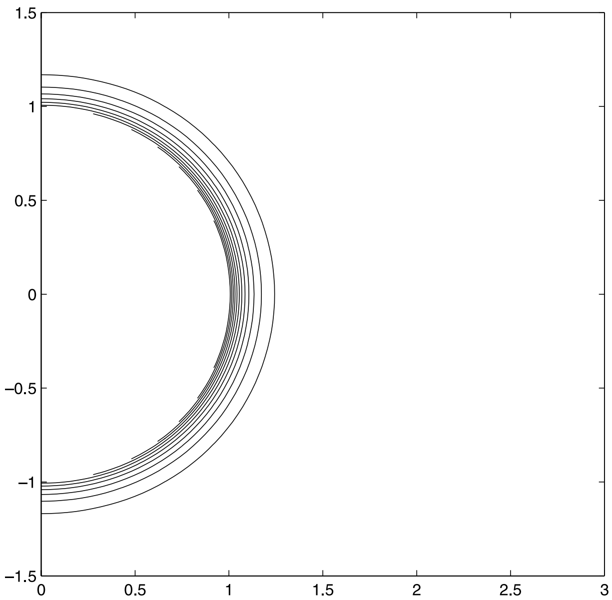

FIG. 2*c*

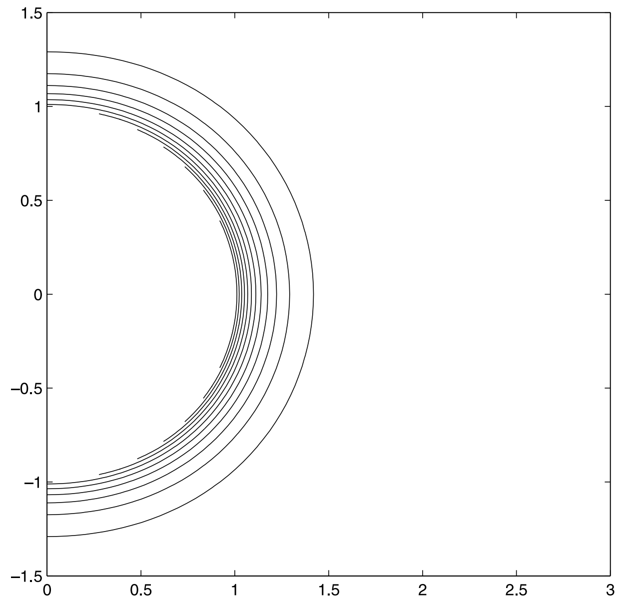

FIG. 2*d*

FIG. 2.—Contours of constant density on the r-θ plane in $r > 1$ associated with the respective fields displayed in the same panel order in Fig. 1. (*a*) $N = 6$, $\gamma_1 = -5$; (*b*) $N = 6$, $\gamma_1 = 5$; (*c*) $N = 6$, $\gamma_1 = 10$; (*d*) $N = 11/3$, $\gamma_1 = 3$.

β_G is typically larger than unity in $r < 2$ showing strong plasma-field interaction in this near region. A smaller amplitude of the negative γ_1 would show a similar radial distribution of β_G with values less than unity, corresponding to a stronger dominance of the magnetic field over the plasma.

Figures 1*d* and 2*d* show the equilibrium state with $\gamma_1 = 3$ in an $N = 11/3$ polytropic atmosphere. This example in the regime of $3 < N < 4$ has an atmospheric temperature large enough so that its equilibrium pressure is significant at large r to stretch the far field into a slow decline with distance. A potential dipole field falls as $1/r^3$ for large r. This nonpotential equilibrium field falls more slowly as $1/r^{8/3}$ for the $N = 11/3$ polytropic atmosphere. An examination of the parameter β_G for this solution shows that it monotonically decreases radially from a value of 1.5 at $r = 1$ to an asymptotic constant value less than unity. This indicates a significant field-plasma interaction for all large distances. The value of β_G falls below unity beyond $r = 2.5$.

For $\gamma_1 > \gamma_{1,\mathrm{crit}} = 8/3$, a magnetic bubble forms with enhanced plasma trapped within. This bubble is too small to be seen in Figure 1*d* at the contour levels used to display the field. For even larger values of γ_1, which we omit to present, the bubble has a more elongated shape than those found in the $N = 6$ polytropic atmosphere because its pressure is significant at all radial distances. Negative values of γ_1 for the polytropic atmospheres with $3 < N < 4$ all involve spherical flux surfaces of $A = 0$ separating a second far atmosphere above it. None of these models are of interest to our numerical study. In the remaining subsections and in the next section we examine how these $N = 6$

and 11/3 poloidal fields are modified when we introduce twist into the equilibrium field by setting $\gamma \neq 0$ and $B_\varphi \neq 0$.

We are interested in the magnetic energy of the $\gamma = 0$ magnetic field:

$$E_0 = \int_{r>1} \frac{1}{8\pi} B^2_{\gamma=0}\, dV = \frac{1}{3}\left[1 + \frac{\gamma_1^2}{(2N-5)(N-1)^2}\right]. \tag{23}$$

If $\gamma_1 = 0$, $\boldsymbol{B}_{\gamma=0}$ is the potential dipole field with $E_0 = E_{\rm pot} = \frac{1}{3}$, the lowest energy for a magnetic field with the prescribed boundary flux at $r = 1$. The energy E_0 is a monotonically increasing function of γ_1^2, independent of the sign of γ_1 despite the difference in topology between fields of γ_1 equal but opposite in sign. Paper I shows that the energy E of a force-free field in $r > 1$ is bounded above by a quantity defined entirely by the boundary flux at $r = 1$. In contrast, the energy E_0 in the presence of field-plasma interaction increases monotonically with increasing γ_1. Given a sufficiently massive atmosphere, its weight can serve to anchor a magnetic field of any magnitude against its natural tendency to expand out of the atmosphere.

3. PLASMA WEIGHT ON TWISTED MAGNETIC FIELDS

We now turn to the general solutions for the boundary value problems posed by equations (17) and (14). These equations describe a polytropic atmosphere of power index N containing a twisted field characterized with a twist index n and a fixed dipolar flux distribution at $r = 1$. We use a numerical solver, described below, to construct families of solutions spanned by the constants γ and γ_1 parameterizing the degrees of magnetic twist and field-plasma interaction. We do not know if the solutions constructed by our solver are, indeed, all the possible solutions to each of the boundary value problems treated. It was pointed out in Paper I that for the force-free fields, i.e., with $\gamma_1 = 0$, there are upper bounds on γ above which no solutions to the boundary value problems exist. If $\gamma_1 \neq 0$, existence of a solution is similarly subject to certain upper bounds on γ, not trivial to derive. For our purpose of discovering basic structural properties as illustrated by explicit solutions, it suffices that our solver is capable of obtaining a diverse continuum of solutions spanned by a finite range of γ for each prescribed γ_1.

Among the numerical solutions we have constructed, the models with polytropic indices $N = 6$ and 11/3 are qualitatively representative of the structural properties we have found. They represent solutions in the regimes $3 < N < 4$ and $N > 4$. In this section we describe some particular solutions for these models as a first step in examining these explicit solutions, beginning with a brief summary of the numerical methods we use and the general physical properties we may anticipate. In the next section we examine a survey of physical properties exhibited collectively by an entire continuum of solutions.

3.1. *Numerical Mathematics*

The numerical elliptic solver, described in the Appendix of Paper I, has been modified to treat the new boundary value problems. We remind the reader that this solver uses (1) Newton's iteration for the treatment of nonlinearity (Fornberg 1988), (2) a pseudospectral representation of the solution for high numerical accuracy (Fornberg 1996), (3) effective far-field asymptotic boundary conditions, and (4) a pseudo–arc length continuation method to ensure the proper continuation of the solution sequence past turning points (for an overview of continuation methods see, for example, Keller 1987; Allgower & Georg 1992). The computational domain is rendered finite by first limiting the unbounded domain to $1 < r < r_\infty$ for some sufficiently large outer radius r_∞ and then stretching that truncated domain with a transformation $s = \log r$ and using the redefined angular coordinate $\eta = \pi/2 - \theta$. We should point out that the source term in equation (17) associated with a cross field current density may dominate in the far regime for $N < 4$, requiring a modification of the far boundary conditions in the original numerical code to account for it.

We pick a fixed value of γ_1 for an atmosphere with a fixed polytropic power index N and a magnetic field of a fixed power-law index n. Then we proceed to construct all the solutions for γ parametrically increasing from zero. The starting point of each solution branch (i.e., sequence) is by definition the purely poloidal field given by equation (20). We then march along the solution branch, where an auxiliary pseudo–arc length parameter has been introduced as the independent variable. The parameter γ then becomes an unknown and is determined along with the solution A by the Newton iterations. This methodology allows us to continue smoothly through all turning points where otherwise the Jacobian would be singular. Computation in each case ends when the solution branch indicates a convergence to a limit solution, a mathematical feature already encountered in Paper I. The boundary value problems for force-free fields in Paper I are, in fact, a special case of our boundary value problems, namely, the case of $\gamma_1 = 0$ for which the starting solution of each sequence is just the potential dipole field.

3.2. *Preliminary Physical Considerations*

In the presence of field-plasma interaction, the energy $E_{\rm total}$ of the atmosphere has three parts, the magnetic energy, the polytropic thermal energy, and the gravitational potential energy, given below, respectively:

$$M(\gamma,\ \gamma_1) = \int_{r>1} \frac{B^2}{8\pi}\, dV, \tag{24}$$

$$U(\gamma,\ \gamma_1) = \int_{r>1} Np\, dV, \tag{25}$$

$$W(\gamma,\ \gamma_1) = -\int_{r>1} \frac{\rho G M_\odot}{r}\, dV, \tag{26}$$

where the thermal energy involves the polytropic index $\Gamma = 1 + 1/N$. A modified derivation of the hydromagnetic virial theorem of Chandrasekhar (1961) for a static atmosphere gives

$$E_{\rm total} = M + U + W = (3 - N)U + \frac{1}{4}\int_{r=1}\left(B_r^2 - B_\theta^2 - B_\varphi^2 - 8\pi p\right)\sin\theta\, d\theta, \tag{27}$$

from which we get an expression for the magnetic energy,

$$E = \int_{r>1} \frac{B^2}{8\pi}\, dV = -\int_{r>1}\left(3p - \frac{\rho G M_\odot}{r}\right) dV + \frac{1}{4}\int_{r=1}\left(B_r^2 - B_\theta^2 - B_\varphi^2 - 8\pi p\right)\sin\theta\, d\theta \tag{28}$$

(see Low & Smith 1993).

In Paper I we have used the notation $E_{\rm total}$ for the total magnetic energy of a force-free field in $r > 1$. Our notation is consistent with that of Paper I. In the absence of field-plasma interaction, we have a force-free field for which $E \equiv E_{\rm total}$ with p and ρ formally set to zero:

$$\begin{aligned} E &= E_{\rm total} \\ &= \frac{1}{4}\int_{r=1}\left(B_r^2 - B_\theta^2 - B_\varphi^2\right)\sin\theta\, d\theta. \end{aligned} \tag{29}$$

In this case the magnetic energy E is bounded above by the integral limited to just the term B_r^2 at $r = 1$ in the integrand. This bound limits the amount of magnetic energy that can be stored in the atmosphere irrespective of how twisted the force-free field is. In the presence of field-plasma interaction, the magnetic energy E, given by equation (28), contains the positive definite term $-W$ associated with the gravitational binding energy of the atmosphere (Low 1999; Hu et al. 2003). So long as this term is sufficiently large, E can be as large as the atmosphere is massive. This is the basic effect of anchoring magnetic flux with mass in the equilibrium atmosphere.

The total azimuthal flux in $r > 1$ is of interest:

$$F_\varphi(\gamma,\ \gamma_1) = \int_{r>1} B_\varphi r\, dr\, d\theta \tag{30}$$

$$= \sqrt{\frac{2\gamma}{1+n}}\int_{r>1} A^{(1+n)/2}\, dr\, \frac{d\theta}{\sin\theta}. \tag{31}$$

The equilibrium fields we examine can all be characterized by the manner in which a total azimuthal flux F_φ is to be distributed in $r > 1$, held in equilibrium by the tension force of a stretched poloidal field anchored to $r = 1$ and by the weight of the atmospheric plasma. These two anchoring effects are countered by the expansive tendency of the magnetic and plasma pressures.

The equilibrium magnetic energy E and the azimuthal flux F_φ are not simply related. By its definition, E generally increases with the physical insertion of more poloidal and azimuthal flux. In our numerical solutions, the amount of poloidal flux anchored to $r = 1$ is fixed by a common dipolar flux at that boundary for all solutions. We are then faced with the interesting question of how much azimuthal flux such a poloidal field may confine and how that confinement might be aided by the weight of a polytropic atmosphere.

The relationship between E and F_φ is made complicated by the fact that for a fixed value of F_φ, E depends on how compactly that total azimuthal flux could be packed spatially. Thus, states of large F_φ are likely to have high magnetic energy, but the precise level of that high energy is greatly dependent on the specific spatial distribution of the azimuthal flux. Of particular interest to us is the formation of an azimuthal flux rope in the axisymmetric atmosphere as a means of compactly packing the azimuthal flux F_φ to the low atmosphere where the anchored poloidal field is strong. With these physical anticipations, we now turn to particular solutions for their explicit properties.

3.3. *The $N = 6$, $\gamma_1 > 0$ Polytropic Atmospheres*

Consider the $N = 6$, $n = 5$ sequence of solutions with γ_1 fixed at the critical value $\gamma_{1,\rm crit} = 5$ shown in Figure 3. We recall that the starting solution of the sequence is the poloidal field given by equation (20) with these parametric values. This starting solution is shown in Figure 1*b*. The left and middle panels of Figure 3 are in the same formats used to represent force-free solution sequences in Paper I. At fixed γ_1, the solution sequence is represented in the left panel of Figure 3 in terms of the magnetic energy E as a multivalued function of the parameter γ. This solution curve curls into a limit point in the manner already seen in the force-free field solution curves of Paper I.

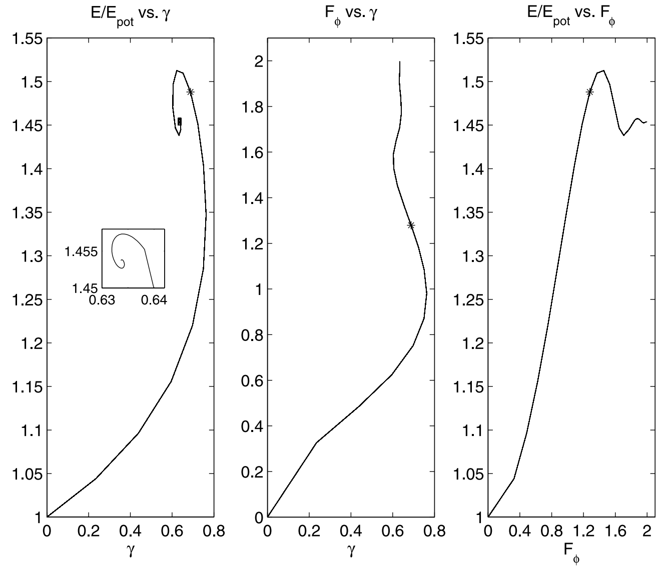

FIG. 3.—Solution sequence for $N = 6$, $n = 5$, $\gamma_1 = 5$ described in the text. The blowup in the left panel shows the neighborhood of the $E(\gamma)$ limit point.

The solution sequence may also be characterized by the total azimuthal flux F_φ in the atmosphere $r > 1$ as a function of γ, shown in the middle panel of Figure 3. While a set of multiple solutions share common values of γ, they have different F_φ. Along the solution curve defined by the $E(\gamma)$ in the left panel, F_φ increases monotonically to reach a maximum value of about 2 corresponding to the limit point of the E representation of the solution curve.

For our purpose in this paper, we combine the two representations of the solution curve to produce a third representation shown in the right panel of Figure 3, displaying E as a function of F_φ along the solution curve. This is physically a more meaningful representation, one that illustrates the variation of the magnetic energy E with a monotonically increasing azimuthal flux F_φ.

The different representations of the solution curve identify two special equilibrium states that capture the basic physics of field confinement in the open atmosphere. The states of maximum magnetic energy and maximum azimuthal flux are not the same. In Figure 3, the maximum energy $E_{\rm max} \approx 1.52$ occurs at a moderate azimuthal flux of $F_\varphi(E_{\rm max}) \approx 1.4$. Magnetic energy, as the integral of magnetic pressure in the atmosphere, is large by virtue of the compact packing of this moderate azimuthal flux into a flux-rope structure near the base of the atmosphere. The maximum azimuthal flux $F_{\varphi,\,\rm max} \approx 2$ occurs at the limit point where $E = E_{\rm limit} \approx 1.45$, slightly lower than $E_{\rm max}$. This larger flux is more diffusely distributed than that in the state at $E_{\rm max}$.

Figure 4 shows the equilibrium state located with an asterisk on the solution curve of Figure 3. Consider the plot of constant flux function A in the r-θ plane. A significant B_φ component directs these lines of force out of that plane in three-dimensional space. The set of constant-A lines completely closed in $r > 1$ describe, with $B_\varphi \neq 0$, a rope of twisted flux running equatorially around the unit sphere. Superimposed on these lines are the dashed lines displaying the contours of constant density,

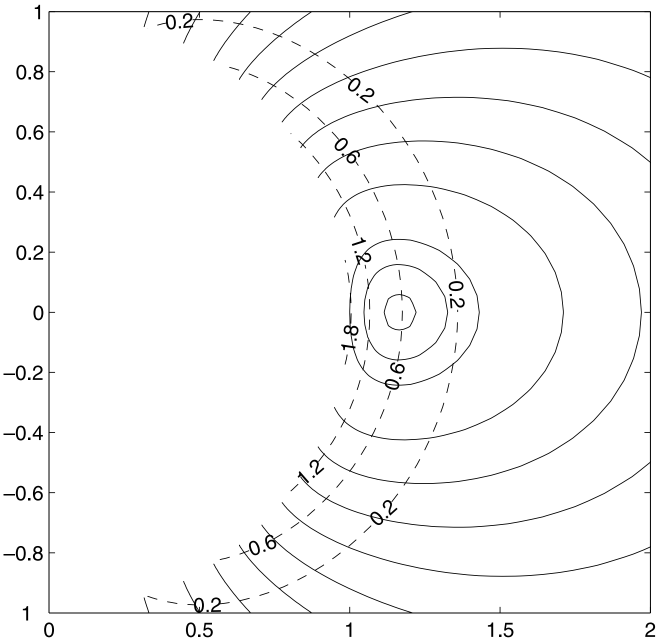

FIG. 4.—Contours of constant A (*solid lines*) and of constant density (*dashed lines*) for the solution located by an asterisk in the sequence shown in Fig. 3. With $B_\varphi \neq 0$, the completely closed contour of A represents an azimuthal rope of twisted magnetic flux.

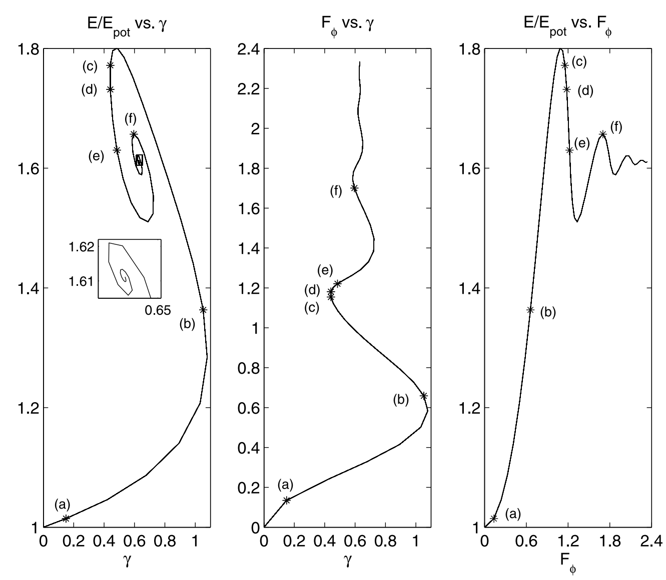

FIG. 5.—Solution sequence for $N = 6$, $n = 7$, $\gamma_1 = 5$ described in the text. The blowup in the left panel shows the neighborhood of the $E(\gamma)$ limit point.

decreasing as an $N = 6$ inverse power of the radial distance (see eq. [16]). The plasma, in its linear dependence on A, is diffusely distributed such that its morphology does not give any hint of the flux-rope topology of the magnetic field. A suitable, highly nonlinear dependence of the plasma distribution on A is required if, combined with its polytropic radial falloff with r, it is to show a morphological correlation between plasma distribution and magnetic field. We have chosen to avoid this complication in this first numerical study.

The field and plasma configuration shown in Figure 4 is characteristic of the solutions in the set shown in Figure 3. The magnetic flux rope is trapped at the base of the atmosphere by two agents: the overlying magnetic field anchored to $r = 1$, as well as the weight of the concentration of plasma in the equatorial region low in the atmosphere. A physical way of interpreting the density distribution in Figure 4 is not to look at it in terms of their global contours of constant density but to follow the fall of density with increasing r along individual field lines of constant A. Along such a line, the Lorentz force has no component and the observed fall of density is associated with a hydrostatic fall of the polytropic pressure to support the plasma weight with its gradient force. This interpretation gives the physical idea of a flux rope trapping a heavy plasma in its lower part, under gravitational stratification and frozen into the field under high electrical conductivity.

It is instructive to compare the solution sequence in Figure 3 with the $n = 5$ force-free field sequence of Paper I matching the same boundary flux at $r = 1$. The two sequences may be regarded to be examples of how a certain amount of azimuthal flux F_φ can be trapped in equilibrium by the poloidal field. For the $n = 5$ force-free field sequence of Paper I, the maximum magnetic energy $E_{\max} \approx 1.35$ occurs at $F_\varphi(E_{\max}) \approx 1.1$ and the maximum azimuthal flux $F_{\varphi,\max} \approx 1.7$ occurs at $E_{\rm limit} \approx 1.33$. The $\gamma_1 = 5$ sequence of the same power index $n = 5$ in Figure 3 shows these two corresponding states to be confining greater azimuthal fluxes at greater energies, as the result of field-plasma interaction. Moreover, the plasma weight permits the configuration of the flux rope to form near $r = 1$, whereas no such structure is found in the force-free field sequence of Paper I.

Figure 5 shows the γ sequence of the $\gamma_1 = 5$ magnetostatic equilibria with a higher $n = 7$ power law for the magnetic twist. The $E(\gamma)$ solution curve shows a more dramatic spiral. The azimuthal flux F_φ is again a monotonically increasing function along the solution curve, reaching a maximum of about 2.3. The curve E as a function of F_φ shows a more pronounced oscillation after E has descended from its maximum value. The two special states are $E_{\max} \approx 1.8$ occurring at $F_\varphi(E_{\max}) \approx 1.1$ and $F_{\varphi,\max} \approx 2.3$ occurring at $E_{\rm limit} \approx 1.61$. Compare this $\gamma_1 = 5$ sequence with the $n = 7$ force-free field sequence of Paper I with the same boundary flux distribution at $r = 1$. For these force-free fields, $E_{\max} \approx 1.6$ occurring at $F_\varphi(E_{\max}) \approx 1$, and $F_{\varphi,\max} \approx 1.65$ occurring at $E_{\rm limit} \approx 1.45$. Both magnetic energy and azimuthal flux of each of these two special states are enhanced by field-plasma interaction, relative to the force-free fields.

The higher index of $n = 7$ implies a spatially more confined azimuthal flux around and within the closed-loop fields near the base where A takes a local maximum. With the linear dependence of p and ρ on A in equation (15), no local maxima in p and ρ are found because of their strong power-law decline with increasing radial distance. As we have pointed out for the $n = 5$ solutions, it is conceivable that a highly nonlinear, complex dependence of p and ρ on A may produce local plasma maxima located within the magnetic flux rope, a complication we postpone to a future study. It should also be pointed out that despite the simple stratification of the plasma, it produces the complexity of a flux rope, not readily anticipated in such nonlinear solutions.

Figure 6 shows the field topologies for representative equilibrium states identified as labeled along the solution curve in Figure 5. Each of these contour plots of constant A contains refined contour intervals, which are not necessarily equispaced, in order to display the fine topological details of the field lines. These field lines point out of the r-θ plane in three-dimensional space with a significant B_φ. We have omitted the contours of constant density in Figure 6 to avoid cluttering the figures. The density is of the simple stratifications morphologically similar to the $n = 5$ states shown in Figure 4.

This set of field topologies should be compared to those of $n = 7$ force-free fields in Paper I. In the force-free field sequence,

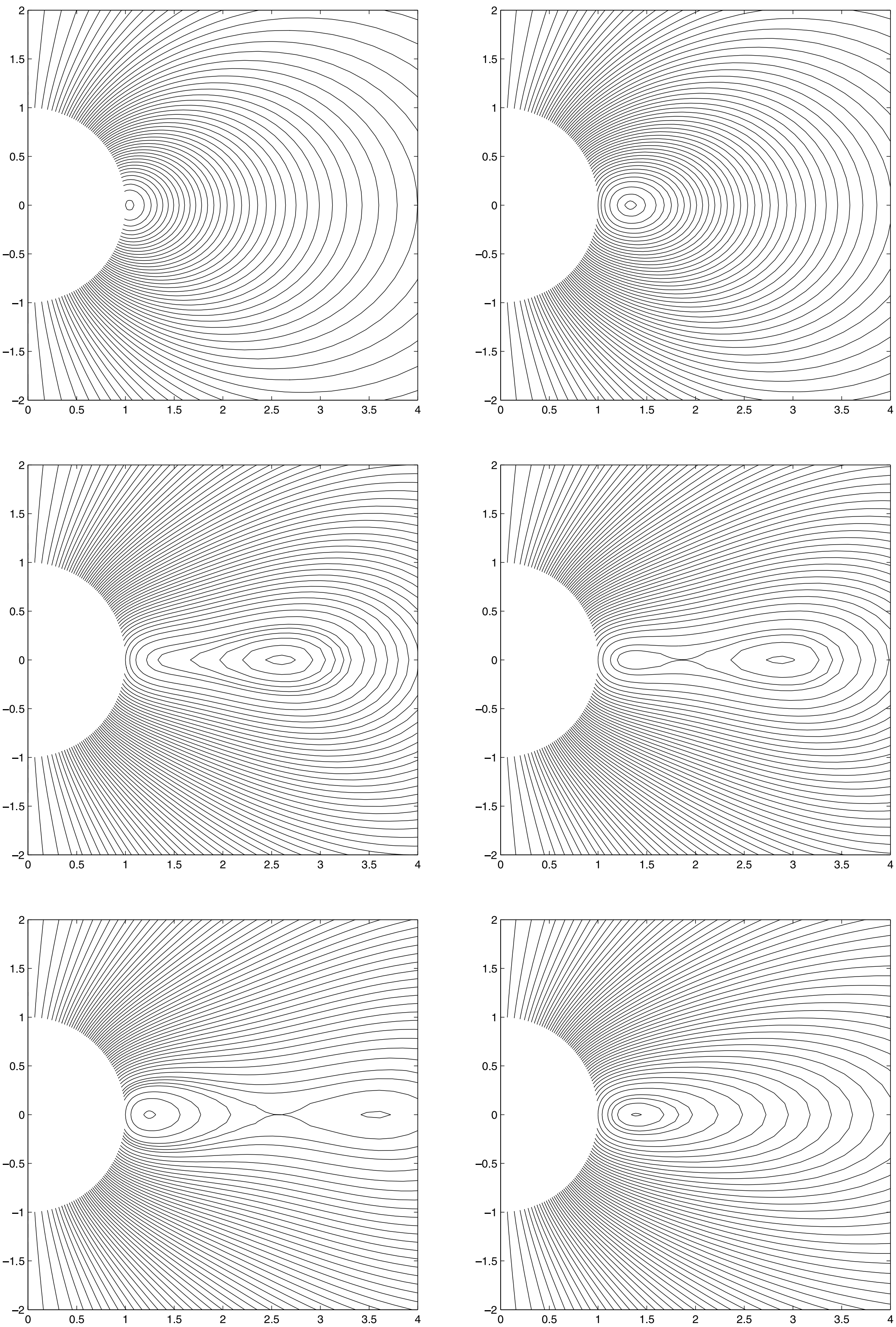

FIG. 6.—Contours of constant A for select solutions identified as labeled in the sequence shown in Fig. 5. Density contours are omitted to avoid cluttering the field-line displays.

magnetic islands of closed lines parametrically form one at a time and move out of the atmosphere. In each case, the flux-rope field counts on the poloidal flux alone to confine the outward expansive tendency of the trapped azimuthal flux F_φ. In the sequence in Figure 6, we find a similar parametric development of magnetic islands, but more than one island can be found. The double islands, each being a local maximum in A, trap a local enhancement in mass, and its weight plays a role in anchoring each flux rope in local equilibrium.

3.4. *The* $N = 6$, $\gamma_1 < 0$ *Polytropic Atmospheres*

Negative values of γ_1 in equation (15) require a fixed β_0 sufficiently large to ensure that p and ρ are positive definite. These solutions describe an equatorial depletion of plasma near the base of the atmosphere. Figure 7 displays the γ sequence of solutions for $\gamma_1 = -5$ of the $N = 6$ polytropic atmosphere, with the twist power-law index $n = 5$. Figure 8 displays representative configurations of constant-A field lines and constant density from this family of solutions. Examine these field-plasma configurations before looking at the solution curve. The equatorial density depletion near the base is characterized with an X-point (i.e., a saddle point). It is the compressed field in this region that holds the region against self-collapse. As a function of θ at fixed radial distance, the depletion is strongest at the equator where $\theta = \pi/2$. Along the equatorial radial line $\theta = \pi/2$, the density increases from the base to a maximum value at the X-point before decreasing with radial distance beyond. It will be interesting but outside the scope of our study to consider the linear stability of such a stratification. Although this stratification is susceptible to the Raleigh-Taylor overturning in the absence of magnetic fields, the curvature force of the magnetic field may suppress this effect. A proper calculation is needed to draw any definite conclusion about the stability of this stratification. A balance between these two effects working in competition to produce an overall stability has been demonstrated elsewhere (Hundhausen & Low 1994).

One might have expected that the depletion of plasma at the base of the atmosphere creates a circumstance that promotes trapping azimuthal flux by the weight of the undepleted upper atmosphere. This expectation is not met in the $n = 5$ solutions in Figures 7 and 8, none of which exhibit a flux-rope topology. This is in spite of the strong $B_\varphi = (1/r \sin\theta)[2\gamma/(n+1)]^{1/2} A^{(n+1)/2}$ at the base near the equator as indicated by larger values of γ for which solutions exist as compared to the $\gamma_1 > 1$ case given in Figure 3. The large field-aligned current associated with larger values of γ in the compressed field near $r = 1$ is associated with a highly sheared dipolar field rather than a flux-rope topology. In the $\gamma_1 > 0$ solutions, the confinement of the azimuthal flux by the poloidal flux is achieved by a distension of the poloidal flux by the pressure force of the azimuthal flux. With an equatorial depletion of plasma parameterized by a negative γ_1, the high plasma pressures in the high latitudes compress the poloidal field into the equatorial depletion region so that only a small amount of poloidal flux penetrates into the far radial distances. This small amount of poloidal flux in the greater space of the upper atmosphere cannot confine much azimuthal flux in that region. The main part of the azimuthal flux is thus compacted into the plasma-depleted region. Both poloidal and azimuthal fluxes in this region are compressed to give the required Lorentz force needed to support the weight of undepleted upper atmosphere. This sets limits to the amount of azimuthal flux to be confined. For an $n = 5$ spread of the azimuthal flux over the poloidal flux function A, these limits are severe. For $N = 6$, $n = 5$, $\gamma_1 = -5$, the solution sequence in Figure 7 is associated with $E_{\max} \approx 1.2$ occurring at $F_\varphi(E_{\max}) \approx 1$ and $F_{\varphi,\max} \approx 1.5$ occurring at $E_{\rm limit} \approx 1.18$, respectively lower than those corresponding energies and azimuthal fluxes of the $n = 5$ force-free fields of Paper I.

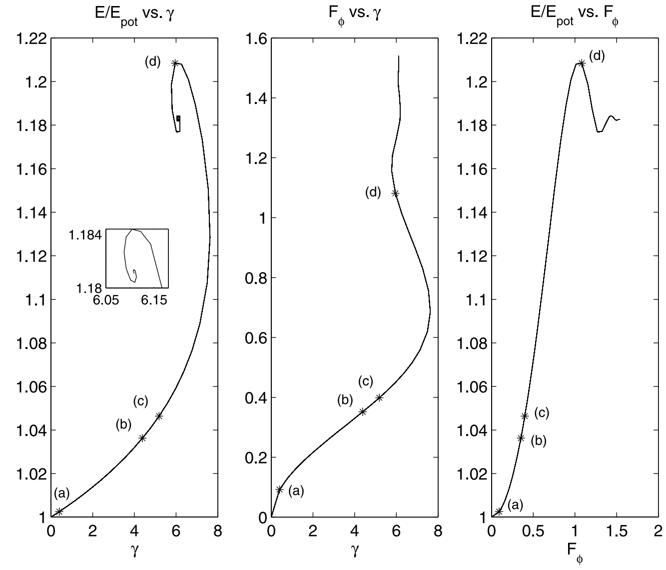

FIG. 7.—Solution sequence for $N = 6$, $n = 5$, $\gamma_1 = -5$ described in the text. The blowup in the left panel shows the neighborhood of the $E(\gamma)$ limit point.

Increasing n from 5 to 7 and keeping $\gamma_1 = -5$, the case shown in Figures 9 and 10 allows for a more compact azimuthal flux rope so that magnetic flux ropes are found in the equilibrium solutions. In Figure 9, the $n = 7$ sequence is characterized with $E_{\max} \approx 1.41$ occurring at $F_\varphi(E_{\max}) \approx 0.8$ and $F_{\varphi,\max} \approx 1.9$ occurring at $E_{\rm limit} \approx 1.29$, showing a better capacity to trap energy and azimuthal flux than the $n = 5$ sequence with the same value for $\gamma_1 = -5$. Compared with the $n = 7$ force-free fields, the equilibrium field in Figure 9 has a lower maximum energy $E_{\max}$ than that of the force-free field but has a greater maximum azimuthal flux $F_{\varphi,\max}$. The former is expected from the compression of the poloidal field by the high plasma pressures in the high latitudes. The latter may be explained in the following way. At $n = 7$, flux ropes allow for a greater packing of the azimuthal flux into the density-depleted region for effective confinement by the weight of the undepleted upper atmosphere. It should be pointed out that the flux ropes of $\gamma_1 = 5$ contain plasma enhancements that resist compression. In contrast, the flux ropes of $\gamma_1 = -5$ are depleted of plasma and can be greatly compressed as is evident in the field configurations shown in Figure 10.

3.5. *The* $N = 11/3$, $\gamma_1 > 0$ *Polytropic Atmospheres*

The $N = 11/3$ polytropic atmosphere has a pressure and density that are significant at large radial distances. This pressure counts on the poloidal field to confine it and therefore, by this consideration alone, we expect less magnetic energy and azimuthal flux to be trapped in equilibrium in the $N = 11/3$ atmosphere compared to the $N = 6$ atmosphere. On the other hand, the added mass at large radial distance can contribute a relatively weak weight to confine the azimuthal flux.

Figures 11 and 12 display the γ sequence for $N = 11/3$, $\gamma_1 = 3$, $n = 5$ showing flux-rope formation aided by the weight of plasma confined to the equatorial region. The maxima $E_{\max} \approx 1.085$ and $F_{\varphi,\max} \approx 1.35$ are respectively lower than the corresponding maxima for the $n = 5$ force-free fields. The poloidal

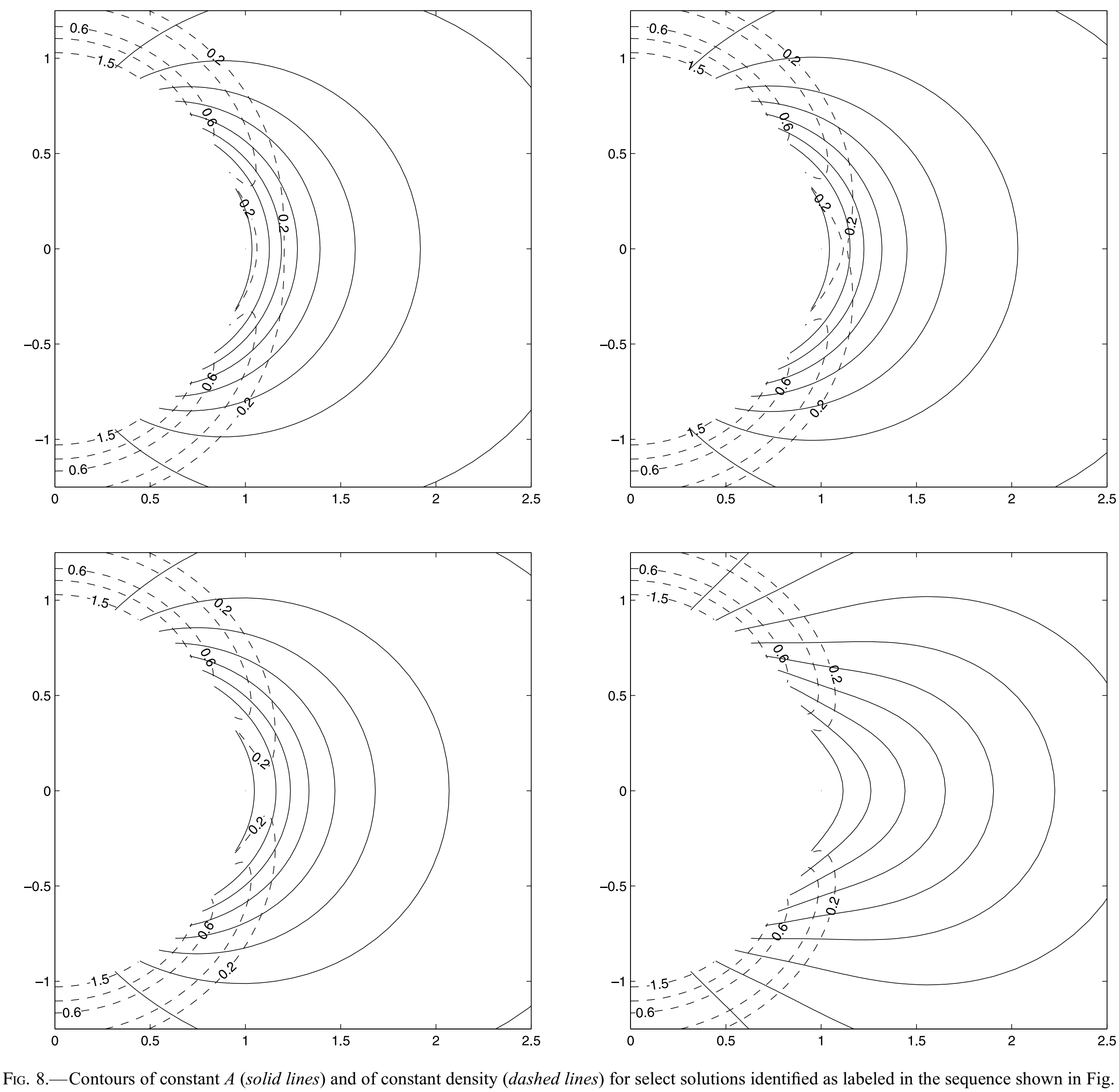

Fig. 8.—Contours of constant *A* (*solid lines*) and of constant density (*dashed lines*) for select solutions identified as labeled in the sequence shown in Fig. 7. The plasma pressures in the high latitudes compress the poloidal flux into the equatorial density depletion region. No completely closed *A* lines are found in the entire sequence of solutions.

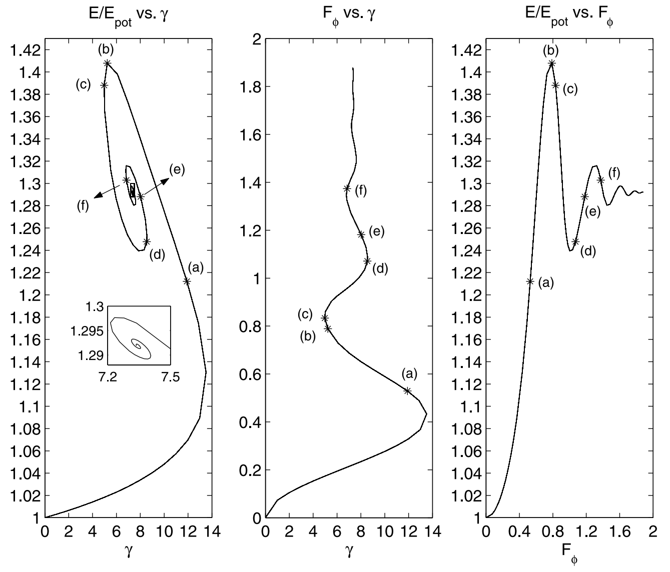

FIG. 9.—Solution sequence for $N = 6$, $n = 7$, $\gamma_1 = -5$ described in the text. The blowup in the left panel shows the neighborhood of the $E(\gamma)$ limit point.

flux is weakened by the strong plasma pressure of this atmosphere and has less confining capability for the azimuthal flux. Flux-rope configurations are found in this sequence such as shown in Figure 12.

Figures 13 and 14 display the γ sequence for $N = 11/3$, $\gamma_1 = 3$, $n = 7$ showing flux-rope formation aided by the weight of plasma confined to the equatorial region. Flux ropes form parametrically in the atmosphere along the solution curve associated with the weak maximum in A in $r > 1$. A different presentation of the flux function A is given in Figure 14 to show its variation in form without dwelling on their detailed structures. Instead of plotting contours of constant A, we horizontally stack together 30 profiles of $A(r,\ \pi/2)$, the solution sequence of A along the equator $\theta = \pi/2$ as a function of $s = \log r$ in the three-dimensional plots shown. The different profiles are labeled by the index k that represents the position on the solution curve with $k = 1$ being the index for the solution for the potential field and monotonically increasing to $k = 30$, the limiting solution in Figure 13. Since F_φ monotonically increases with k, the graphs reveal the subtle structural changes in the equatorial profile of the flux function as the azimuthal flux continually increases. Parametrically local maxima and inflection points form and disappear. Better confinement is produced by the increased power-law index of $n = 7$ as compared to $n = 5$. The maxima are $E_{\max} \approx 1.22$ and $F_{\varphi,\max} \approx 1.96$, respectively. The maximum $E_{\max}$ is lower than that found for the $n = 7$ force-free fields, but the maximum $F_{\varphi,\max}$ is larger than that found for the $n = 7$ force-free fields. In the latter, plasma weight distributed over large radial distances serves as an additional confinement of the azimuthal flux.

4. THE ENERGY AND FLUX OF THE $n = 7$ TWISTED MAGNETIC FIELDS

The particular solutions at fixed values of γ_1 in Figures 3–14 give us a first acquaintance with the properties of the $n = 5$ and 7 equilibrium fields in the $N = 6$ and 11/3 polytropic atmospheres. This acquaintance prepares us for the discussion in this section of two properties, magnetic energy storage and azimuthal flux confinement. This discussion, centered on a collective consideration of the $n = 7$ equilibrium fields, takes us on the next step to the physical discussion of the real solar corona in § 5.

4.1. *The Aly Energy*

The preoccupation with magnetic energy E rather than the total energy $E_{\rm total}$ of the atmosphere, which includes the plasma energy, comes from two considerations. Under the condition of high electrical conductivity in the solar corona, a magnetic field would evolve while retaining its twist, measured in terms of the relative magnetic helicity, brought along with the field during its emergence into the atmosphere (Berger 1984; Taylor 1974; Amari et al. 2000, 2003a, 2003b; Fan 2001; Fan & Gibson 2003, 2004; Gibson et al. 2004; Magara 2004; Manchester et al. 2004; Lites et al. 1995; Lites & Low 1997; Low 1994, 1996, 2001; Rust 1994; Zhang & Low 2001, 2003, 2005). Suppose this field evolves in the corona without being ejected out of the corona and without more flux or helicity injected into it after its emergence. During its quiescent phase of existence, the field would assume equilibrium states conserving its relative magnetic helicity but containing a variable amount of plasma trapped in the field. The flows along field lines anchored to the atmosphere below the corona can readily bring mass into or out of the corona to achieve each state of field equilibrium, depending on the circumstance. Hence, the energy contributed by the plasma is incidental whereas the magnetic energy E has the physical significance as described below in the context of solar CMEs.

The question we consider is whether the magnetic energy E may exceed the Aly (1984, 1991) energy $E_{\rm Aly}$ defined to be the least of the energies of all the opened fields sharing the same boundary flux of a given closed equilibrium field. This question remains of primary interest in the presence of field-plasma interaction because the field is believed on observational grounds to be the principal driver of an expulsion process producing a CME. Therefore, the preeruption equilibrium field must satisfy the necessary condition $E > E_{\rm Aly}$ in order to account for the considerable magnetic energy retained in the field that is stretched opened and left anchored to the base of the corona by the outgoing CME (Aly 1984, 1991; Low & Smith 1993; Wolfson 1993, 2003).

Equilibrium fields involving a field-plasma interaction may have a negative total energy $E_{\rm total}$ because the potential energy is negative for Newtonian gravity (Low & Smith 1993; Wolfson & Dlamini 1997; Fong et al. 2002; Low et al. 2003). The condition $E_{\rm total} < 0$ merely indicates that the atmosphere does not have sufficient energy to take all its trapped plasma out to infinity and is stable against such an expulsion. Most quiescent coronal magnetic structures probably are stable in this manner. A state with $E > E_{\rm Aly}$ but $E_{\rm total} < 0$ is of considerable interest. Its trapped mass plays two roles, that of providing stability during the quiescent existence of the coronal structure and the other of triggering a CME-like expulsion by mass draining off the magnetic field in the course of evolution. As the mass drains off, the field does not attain a potential state if it is endowed with a considerable conserved field helicity. In other words, a certain amount of magnetic energy is trapped with that conserved helicity (Low 1994, 1996, 2001; Zhang & Low 2005). If the trapped magnetic energy is large enough for the field to open up spontaneously, the field will then do so, expelling not all the original mass in its equilibrium state but only the part of the mass that has not drained to the atmosphere below.

The energetic requirement of a CME event is more demanding than that expressed by $E > E_{\rm Aly}$. Consider a common CME with a mass of 5×10^{15} g moving at a median speed of about 500 km s^{-1}. Its kinetic energy is about 6×10^{30} ergs. The gravitational escape speed in the low corona is of the order of 500 km s $^{-1}$. This indicates that to expel the CME out of the corona requires another

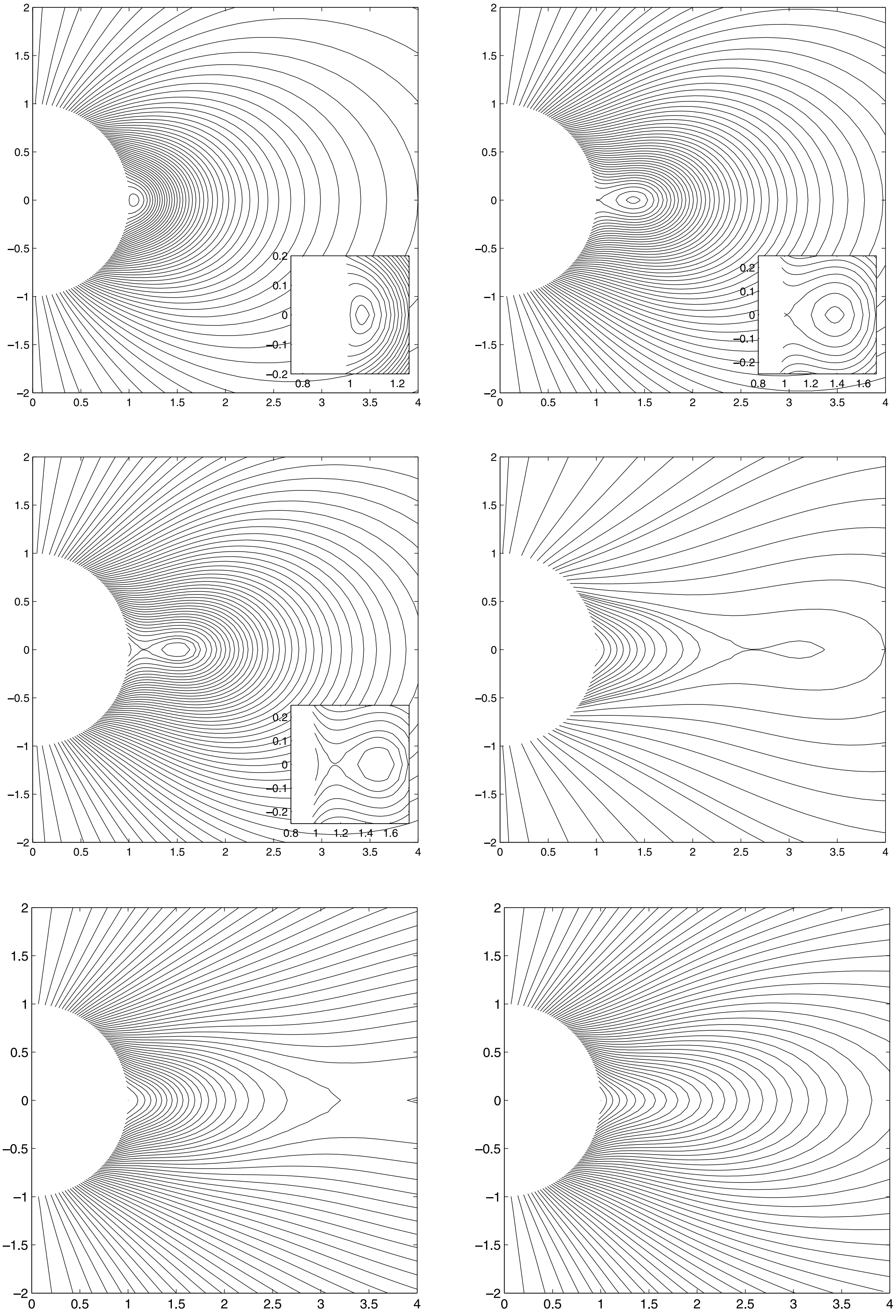

FIG. 10.—Field topologies of select solutions identified as labeled in the sequence shown in Fig. 9. The inserts show localized flux-rope structures.

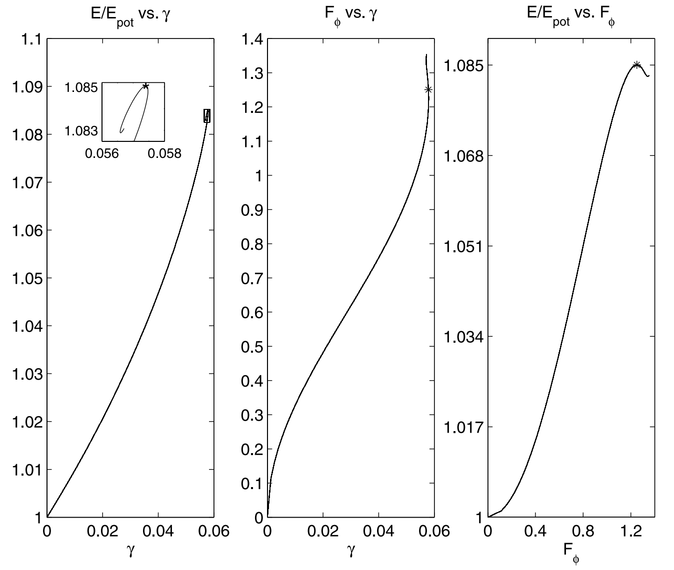

FIG. 11.—Solution sequence for $N = 11/3$, $n = 5$, $\gamma_1 = 3$ described in the text. The blowup in the left panel shows the neighborhood of the $E(\gamma)$ limit point.

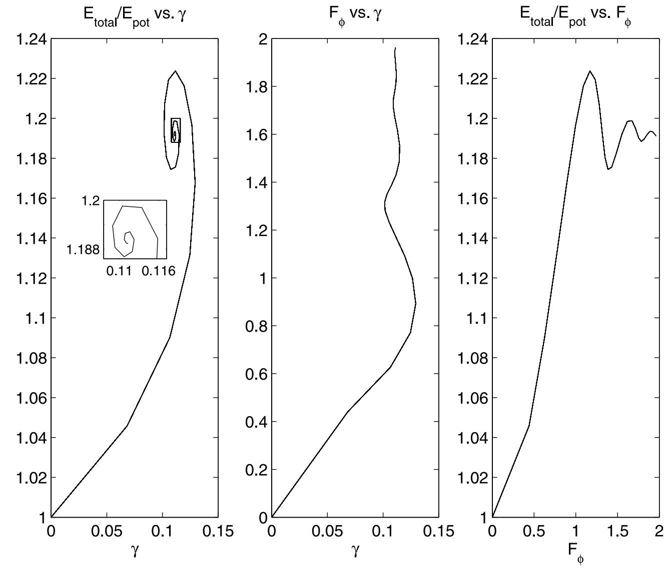

FIG. 13.—Solution sequence for $N = 11/3$, $n = 7$, $\gamma_1 = 3$ described in the text. The blowup in the left panel shows the neighborhood of the $E(\gamma)$ limit point.

6×10^{30} ergs to account for the work done against gravity, liberating a total energy of about 1.2×10^{31} ergs. This is clearly a lower limit since we have not accounted for the energy of the magnetic flux carried out in the CME. Observation has shown that the magnetic field opened by a CME typically will reclose by magnetic reconnection that is interpreted to release the magnetic energy residing in the opened magnetic field. This energy is of the order of a few times 10^{31} ergs in the form of an X-ray flare, usually of the two-ribbon type (Hiei et al. 1993; Tripathi et al. 2004; Amari et al. 2000, 2003a, 2003b). This phenomenology suggests a rule of thumb that a preeruption equilibrium field needs to store energy to account for two comparable pieces: the energy trapped in the stretched-open field left by the CME and the kinetic and gravitational potential energy of the CME.

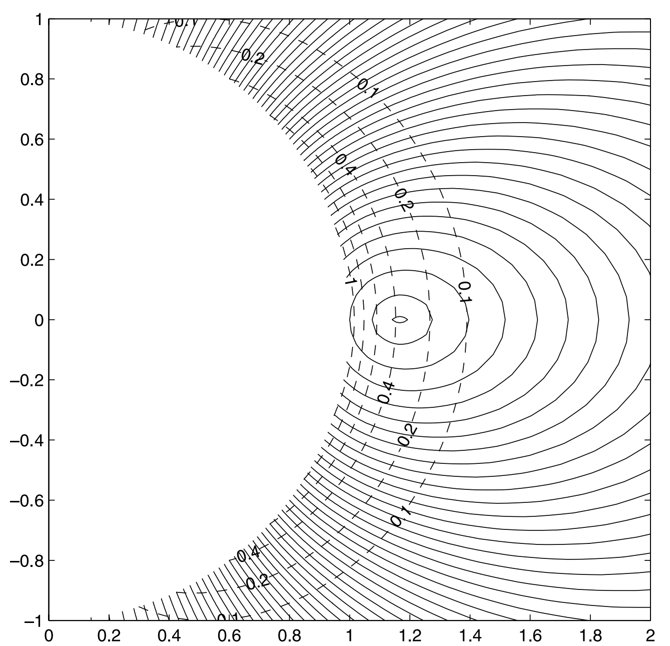

FIG. 12.—Contours of constant A (*solid lines*) and of constant density (*dashed lines*) for the state with $E = E_{\max}$ in the solution sequence shown in Fig. 11. The completely closed A line represents an azimuthal rope of twisted magnetic flux.

Given an equilibrium magnetic field with magnetic energy E, we introduce the two energy differentials $\Delta E = E_{\rm Aly} - E_{\rm pot}$ and $\delta E = E - E_{\rm Aly}$. There are many examples of a CME accelerating to full motion in the upper corona 5–10 minutes before the associated soft X-ray flare commences, the latter interpreted to be heating produced by magnetic reconnection to reclose a global field opened by the CME (Hundhausen 1997, 1999). Such a CME suggests an identification of ΔE and δE with the associated flare and the CME, respectively. The tacit assumption is that the CME in this case is a magnetic flux rope breaking confinement by its expansive force, to leave behind the anchored part of the global field in a fully opened state containing ΔE trapped in a current sheet (see Fig. 3 in Low 2001). If we accept that a CME and its associated flare separately liberate a comparable amount of energy of the order of 10^{31} ergs, we may loosely set $\Delta E = \delta E$ to postulate that a CME-producing magnetic field is required to have an energy of the order of $E_{\rm CME} \approx E_{\rm pot} + 2\Delta E$. For the dipolar fields satisfying the boundary conditions given by equation (14), $E_{\rm Aly} \approx 1.66 E_{\rm pot}$ and $\Delta E \approx .66 E_{\rm pot}$ and the storing energy would then be on the order of $E_{\rm CME} \approx 2.32 E_{\rm pot}$.

A force-free field with its energy given by equation (29) is absolutely bounded above by

$$E_{\rm abs} = \frac{1}{4}\int_{r=1} B_r^2 \sin\theta \, d\theta. \qquad (32)$$

For the dipolar fields satisfying the boundary conditions given by equation (14), $E_{\rm abs} = 2E_{\rm pot}$, showing that the postulated energy $E_{\rm CME}$ cannot be met with a force-free field. Our purpose in this section is to analyze how well the energy $E_{\rm CME}$ may be met with the $n = 7$ equilibrium field. This analysis is physically germane to the dynamics of the above class of CMEs. It is also a demonstration, interesting in its own right, on the mechanics of energy storage in the presence of field-plasma interaction. On the other hand, we must not overlook certain important general

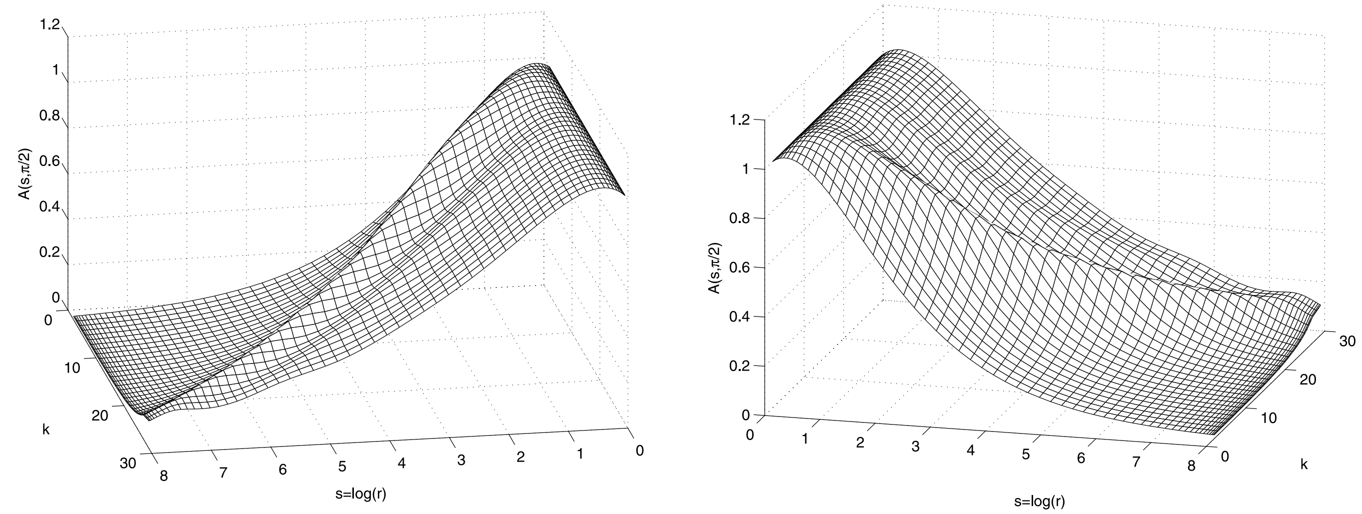

FIG. 14.—Three-dimensional display of 30 profiles of $A(r,\ \theta = \pi/2)$ along the solution sequence shown in Fig. 13, viewed from two perspectives. The axes are labeled $s = \log r$, the radial distance expressed in terms of the exponentially stretched coordinate used in the computation, and k is simply an index to represent the position on the solution curve with $k = 1$ being the index for the solution for the potential field and monotonically increasing to $k = 30$, the limiting solution in Fig. 13.

issues of energy storage, which are briefly discussed in the next subsection. These issues motivate and set qualifications on the results we have obtained.

4.2. *General Issues of Magnetic Energy Storage*

The magnetic energies of an idealized axisymmetric atmosphere cannot be directly related to the observed energies of real flares and CMEs. Let us consider this issue in the case of a force-free magnetic field. Data interpretation suggests that the polar magnetic fields of the Sun are about 10 G (Hundhausen 1977). Set $B_r = 10$ G at $r = R_\odot$, $\theta = 0$ to get $B_0 = 5$ G. Then, $E_{\rm pot} \approx 2.9 \times 10^{33}$ ergs, $E_{\rm Aly} \approx 4.7 \times 10^{33}$ ergs, and $\Delta E \approx 1.9 \times 10^{33}$ ergs. If we accept that for force-free fields δE can be as large as only 8% of $E_{\rm Aly}$, then $\delta E \approx 3.8 \times 10^{32}$ ergs (Hu et al. 2003; Li & Hu 2003; Wolfson 2003; Paper I). These numbers need to be scaled down to account for the actual sizes of CMEs. Although CMEs are large-scale eruptions, they are limited in lateral extent. That is, they are not eruptions of the entire corona. Typically, a fully developed CME viewed against the sky may have latitudinal extent of as much as 90°, but they may originate from low in the corona with an extent of only 20° (see a well-observed event reported in Zhang et al. 2004). Taking the base area of such a CME as a fraction of the entire solar surface, the above energies are scaled by a factor of about 10^{-2} to give $E_{\rm pot} \approx 2.9 \times 10^{31}$ ergs, $E_{\rm Aly} \approx 4.7 \times 10^{31}$ ergs, $\Delta E \approx 1.9 \times 10^{31}$ ergs, and $\delta E \approx 3.8 \times 10^{30}$ ergs. The combined energy in excess of $E_{\rm pot}$, i.e., $\Delta E + \delta E$, is approximately 2.3×10^{31} ergs.

To the extent that such a simple scaling of energies is indicative of the physics, a force-free flux rope may store energy sufficient to account for the expected total energy of a CME-flare event. That the above δE is 5 times smaller than ΔE is troubling since there are many CMEs that have very weak X-ray flare associations (Hundhausen 1999, 1997; Burkepile et al. 2004). A weak flare is here taken in the sense that its total energy output is of the order of 10^{29} ergs and is not detected above the background soft X-ray produced by the full-disk Sun. Such a flare may be observed in soft X-ray solar images, but its total output is in the noise of the full-disk output (Burkepile et al. 2004). Of particular note is that this type of CME can be massive and energetic. The event of 1989 March 18 observed by the Solar Maximum Mission Coronagraph is a CME with a mass of 10^{16} g moving at a speed of about 750 km s^{-1}, carrying away kinetic and potential energies summed up to about 4.5×10^{31} ergs (Hundhausen 1997). This CME is not associated with a flare detectable against the full-disk soft X-ray output of *GOES*.

The observations of Zhang et al. (2001, 2004) provide some new insight into the complexity of CME-flare relationship. These authors found that some fast CMEs observed with *SOHO* LASCO, having speeds in excess of 500 km s^{-1}, are associated with soft X-ray flares that commence at the CME onset with a close correlation between the CME acceleration and X-ray output. These authors also confirm the phenomenon of a slow CME that has no detectable soft X-ray flare. Their fast-CME observations suggest that for such events, magnetic reconnection of the field opened by the CME takes place during the acceleration phase of the CME so that our separation of the flare, ΔE, and CME, δE, energies is not justified in this case. A part of ΔE liberated by reconnection may thus contribute to driving the CME (Anzer & Pneuman 1982; Chen & Shibata 2000; Low & Zhang 2002). The magnitude of such a contribution is an unknown to be determined by future observations and hydromagnetic calculations. The nature of the actual reconnection is crucial to such a determination. Magnetic twist or helicity can escape as Alfvén waves along a fully opened magnetic field. But, if the stretched field begins to reconnect before it becomes fully open, a part of the magnetic twist may be trapped in the postflare relaxed magnetic field. This final nonpotential state implies that not all of ΔE can be liberated, further complicating the physics of such a process.

What is intriguing about the CME energy is that it is ordered energy: kinetic energy and work done against solar gravity, not to mention the energy of the large-scale flux carried away within the CME. In contrast, flare energy is liberated as dissipative heat, which is the reason for identifying it with ΔE due to the presence of a current sheet in the opened magnetic field. CMEs with weak-flare associations suggest the possibility of liberation of a large amount of ordered energy with little reconnection-generated heat, implying a preeruption magnetic field with δE being larger than ΔE in our idealized model. Such a situation exists if there is field-plasma interaction. With this motivation, we proceed to examine our $n = 7$ solutions for the circumstances under which $\Delta E = \delta E$. That is, we formally accept the energy requirement set by $E_{\rm CME} \approx E_{\rm pot} + 2\Delta E$ and analyze how close E may get to $E_{\rm CME}$, keeping in mind that this is a basic physics demonstration

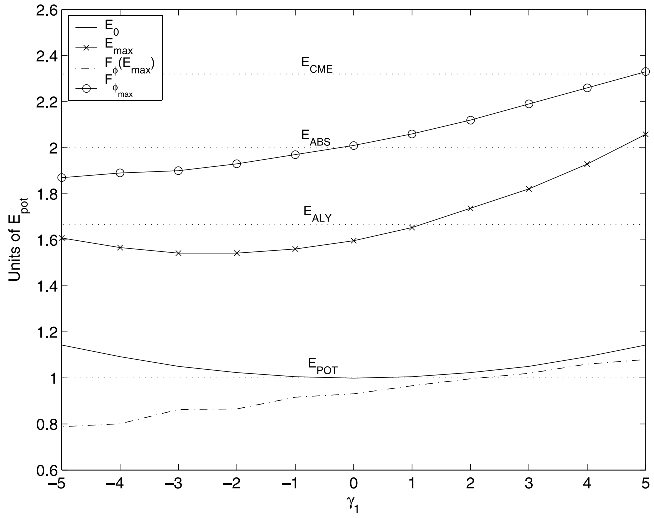

FIG. 15.—Graphs of $E_{\max}$, E_0, $F_{\varphi,\max}$, and $F_\varphi(E_{\max})$ as a function of γ_1 for $N = 6$ and $n = 7$. Energy is given in units of $E_{\rm pot}$, and flux is given in dimensionless units with $B_0 = r_0 = 1$.

in its own right. The results obtained should be held with the qualifications described above.

4.3. *The Magnetic Energy of the $N = 6$, $n = 7$ Twisted Fields*

Recall that $E_{\max}$ is the maximum magnetic energy of the equilibrium fields making up a γ sequence of twisted fields for a fixed γ_1. Figure 15 is a plot of $E_{\max}$ in a range of the fixed values of γ_1 for the $N = 6$ polytropic atmosphere, showing a minimum centered at about $\gamma_1 = -3$. Also plotted is the energy $E_0(\gamma_1)$ of the $\gamma = 0$ poloidal equilibrium magnetic field, given by equation (23), from which each γ sequence starts. The graph $E_0(\gamma_1)$ is symmetrical about $\gamma_1 = 0$ because it is independent of the sign of γ_1. Indicated with the dotted lines are the energy levels $E_{\rm pot}$, $E_{\rm Aly}$, $E_{\rm CME}$, and $E_{\rm abs}$. For each given value of γ_1, the difference $E_{\max} - E_0$ is the maximum energy added to the field through its twist or through its field-aligned current density. In other words, $E_{\max}(\gamma_1) - E_0(\gamma_1)$ is the maximum energy by a maximization over all twisted fields with a fixed γ_1. The divergence between the graphs of $E_{\max}$ and E_0 for increasing γ_1 shows that the atmosphere as a whole is field dominated for larger γ_1.

Of interest are the following observations: (1) E_0 is a slowly increasing function of $|\gamma_1|$; (2) $E_{\max}$ exceeds the thresholds $E_{\rm Aly}$ and $E_{\rm abs}$ at $\gamma_1 > 1.5$ and $\gamma_1 > 5$, respectively; and (3) the minimum of $E_{\max}$ shows that plasma depletion characterized with $\gamma_1 < 0$ lowers this maximum energy stored in the twisted magnetic fields, so that none of the $\gamma_1 < 0$ states clear the threshold of $E_{\rm Aly}$. In particular, the $\gamma_1 = 0$ force-free fields, with $n = 7$ in this set, do not clear the threshold of $E_{\rm Aly}$. In Paper I it was shown that the $n = 9$, more tightly wound-up, force-free fields do clear the threshold of $E_{\rm Aly}$. This suggests that for the $n = 9$ twisted fields, the $E_{\max}(\gamma_1)$ graph would have properties similar to that shown in Figure 15 but shifted higher in value with better clearance of the thresholds of $E_{\rm Aly}$ and $E_{\rm abs}$. It should be pointed out that the threshold $E_{\rm CME}$ is loosely defined to include equal amounts of stored magnetic energies for the CME and its associated flare. The two phenomena may have a variable ratio of energies between them so that $E_{\rm abs}$, of the same order of magnitude as $E_{\rm CME}$, could also serve as a reasonable threshold of energy requirement for a CME/flare event.

Bear in mind that the state of maximum energy does not coincide with a state of maximum azimuthal flux. We make this point by plotting in Figure 15 $F_\varphi(E_{\max})$, the total azimuthal flux in the state when $E = E_{\max}$, and the maximum azimuthal flux $F_{\varphi,\max}$ of each γ sequence generated for a fixed γ_1. Both curves are monotonically increasing in the range of γ_1 of the plot, from negative to positive values. For each γ_1, $E = E_{\max}$ occurs typically with a total azimuthal flux $F_\varphi(E_{\max})$ of about half of $F_{\varphi,\max}$. The large magnetic energy $E_{\max}$ is due to a packing of the flux $F_\varphi(E_{\max})$ into a compact flux rope at the base of the atmosphere. The atmosphere within the set of $n = 7$ solutions is capable of storing twice as much azimuthal flux, as indicated by the ratio of $F_{\varphi,\max}$ to $F_\varphi(E_{\max})$, but only in a more diffused distribution at an energy lower than $E_{\max}$.

Negative values of γ_1 correspond to density depletion in the equatorial region of the lower part of the atmosphere. Both the poloidal and azimuthal fluxes are compressed into this depletion region in order to partially support the undepleted upper atmosphere with their Lorentz force. As we saw from the particular solutions in § 3, this limits the amount of azimuthal flux that can be trapped in the atmosphere. Magnetic flux ropes do form in this regime in γ_1 with the flux rope depleted of plasma as opposed to an enhancement in the region of $\gamma_1 > 0$. These characteristic features of equilibrium underly the shift of the minimum in the graph of $E_{\max}(\gamma_1)$ to the left of $\gamma_1 = 0$ in Figure 15, as well as the monotonically lower values of $F_\varphi(E_{\max})$ and F_φ for increasingly negative values of γ_1.

4.4. *The Magnetic Energy of the $N = 11/3$, $n = 7$ Twisted Fields*

In the $N = 11/3$ atmosphere, plasma pressure is significant for all radial distances, distending the far field into a nonpotential state. This large pressure head at far radial distances relies on the poloidal field for confinement. The capability of the poloidal field to also confine the azimuthal flux is correspondingly reduced. This property can be seen in the decrease of $E_{\max}$ and $F_{\varphi,\max}$ to their respective minima as γ_1 increases from 0, shown in Figure 16. The $n = 7$ force-free field, with $\gamma_1 = 0$, falls short of the threshold $E_{\rm Aly}$. With added polytropic pressure as γ_1 increases from zero, the amount of azimuthal flux is reduced to enable the poloidal flux to accommodate the addition of plasma pressure significant at all radial distances. The eventual monotonic increase of $E_{\max}(\gamma_1)$ for $\gamma_1 > 1.5$ is due to the formation of

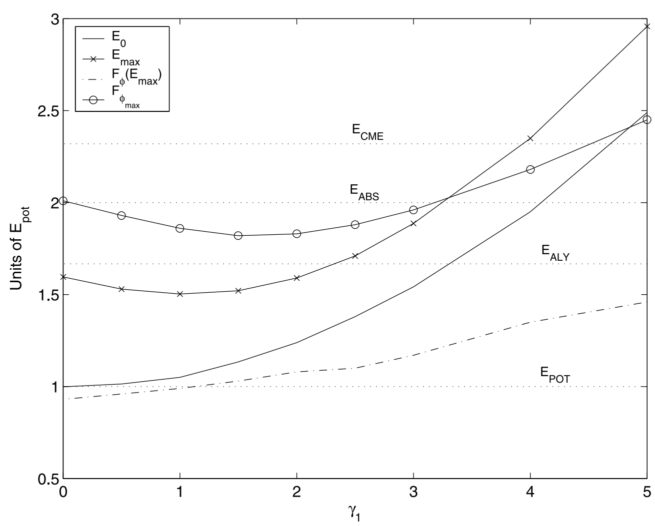

FIG. 16.—Graphs of $E_{\max}$, E_0, $F_{\varphi,\max}$, and $F_\varphi(E_{\max})$ as a function of γ_1 for $N = 11/3$ and $n = 7$. Energy is given in units of $E_{\rm pot}$, and flux is given in dimensionless units with $B_0 = r_0 = 1$.

a plasma-loaded flux rope at the base of the atmosphere to anchor the global field. For $\gamma_1 > 2$, $E_{\rm max}$ is approximately shifted by a positive constant from E_0. That is, the twist in the field introduces a fixed amount of magnetic energy, in contrast to the divergence of $E_{\rm max}$ from E_0 for the $N = 6$ atmosphere shown in Figure 15. With sufficient mass added to both atmospheres, $E_{\rm max}$ can exceed all the thresholds marked by dotted lines in Figures 15 and 16.

4.5. *Strict Bounds on the Total Azimuthal Flux*

Paper I suggests that the axisymmetric, power-law force-free fields may not have a total azimuthal flux in excess of some bound fixed by the flux function A given at $r = 1$. This is only a conjecture because we have no rigorous assurance that our solver is exhaustive in determining all the solutions to the boundary value problems treated. We will take up this conjecture in a follow-up study, but its relevance to the energy properties in Figures 15 and 16 is worthy of a brief discussion.

Paper I pointed out that the force-free field in a finite domain bounded by a rigid wall can have any prescribed total energy E by taking the field to be sufficiently twisted. In contrast, the energy of a force-free field in the unbounded domain $r > 1$ is, by the Chandrasekhar virial theorem, strictly bounded by $E_{\rm abs}$ fixed by A on $r = 1$, completely independent of the twist of the field. In unbounded space, a force-free field has to self-confine against outward expansion. The physical expectation remains that the more greatly twisted a field is, the more energy it should have, suggesting that if a force-free field in $r > 1$ is too highly twisted, by some quantitative measure of that twist, it will be too energetic to be in equilibrium. Denied equilibrium, such a field must expand to expel a part of the flux out to infinity, taking some twist with it. This expulsion leaves behind a less twisted, anchored part of the field to find equilibrium otherwise forbidden. This interesting possibility has been suggested to be the basic dynamical origin of CME eruptions (Low 1994, 1996, 2001; Zhang & Low 2005).

The relative magnetic helicity defined in Berger & Field (1984) is a quantitative measure of magnetic twist. For our purpose, we use the alternative to measure twist by the amount of total azimuthal flux F_φ in $r > 1$ for a given poloidal flux anchored to $r = 1$. Figures 15 and 16 show that field-plasma interaction is a means of trapping both magnetic energy and azimuthal flux at levels beyond those attainable in pure force-free fields. The amount of plasma in the atmosphere can be variable, being an incidental consequence of the exchange of mass between the solar corona and the high-density atmosphere below. On the other hand, the amount of azimuthal flux that has entered the corona is not easy to destroy, even in the presence of magnetic reconnection, because of the high electrical conductivity of coronal plasma (Berger 1984). Thus, the drainage of a plasma, trapping an excessive amount of azimuthal flux in the corona, back to the dense atmosphere below would leave behind this trapped azimuthal flux. The stage is then set for the field-dominated corona to expand in a CME-like expulsion to rid the field of its excessive azimuthal flux.

The nonlinear equilibrium equations are formidable even under the simplifying idealization of axisymmetry (Courant & Hilbert 1963). Our numerical solutions serve to illustrate basic hydromagnetic properties without implying that their distributions of plasma and magnetic field are realistic representations of the solar corona. These properties are of two classes, those that suggest fundamental processes like the above limit on azimuthal flux in axisymmetric fields and others that relate to realistic properties of the corona idealized in simple models. We now turn to the latter class to relate our results to the real corona.

5. SUMMARY AND CONCLUSIONS

We first describe the observed corona and then relate our numerical solutions to several aspects of the physical picture described.

5.1. *The Observed Corona*

The quiescent magnetic fields of the order of 10 G or stronger are largely force-free near the base of the solar corona but not force-free above a height of about 1–1.5 $R_\odot$ from the base (Hundhausen 1977; Li et al. 1998; Sun & Hu 2005). All field lines extending to such heights are combed by the solar wind to open into interplanetary space (Pneuman & Kopp 1971). Below such a height, closed fields that are anchored at both ends to the coronal base trap plasmas in quasi-static equilibrium. These often take the form of helmet-shaped coronal structures, such as those in the photograph of the 1988 March 18 total solar eclipse in Figure 17. This picture registers Thomson-scattered light originating from the eclipsed Sun. Brightness in the image represents high columnar plasma density in the optically thin corona (Gibson et al. 2003). The conspicuous large helmet at the northwest solar limb in this picture shows a coronal helmet with a three-part structure. These are the high-density main part of the helmet, the low-density, small, dark cavity at the helmet base, and, the knotlike, bright quiescent prominence in the cavity.

Observations have shown that the median 5×10^{15} g CME mass is largely of coronal origin. Many CMEs are observed to erupt from a preexisting coronal helmet (Hundhausen 1999). The three-part structure of the helmet is preserved during eruption to form a bright, leading dense shell of the CME, a dark cavity, and the erupted prominence inside the cavity (Illing & Hundhausen 1986; Gibson & Low 1998, 2000; Cremades & Bothmer 2004; Ciaravella et al. 2000; Dere et al. 1999). The CME event of 1980 August 18 displayed in Low (2001) is an example. Observations and models suggest that the mass of a quiescent prominence lies in the range 10^{14}–10^{16} g (Schmahl & Hildner 1977; Rusin & Rybansky 1982; Gopalswamy & Hanaoka 1998; Lipscy 1998; Patsourakos & Vial 2002; Gilbert et al. 2005; Fong et al. 2002; Low et al. 2003). Masses comparable to the median CME mass of 5×10^{15} g are gravitationally significant. During eruption, a larger part of the prominence is drained back to the lower atmosphere while a smaller part is expelled as the core of the CME (see the discussion and references in Low et al. 2003).

Unfortunately, coronal fields on the scale of the helmet cannot be detected readily, although progress toward achieving that has been made (e.g., Judge et al. 2002; Kuhn et al. 1999). Prominence observations and theory suggest that the prominence is a horizontal, lengthy, plasma condensation suspended in a low-density, larger sized, horizontal magnetic flux rope (Leroy et al. 1983; Leroy 1989; Bommier 1998; Lopez Ariste & Casini 2002; Low & Hundhausen 1995). This flux rope is suspended low in the corona running parallel to a magnetic polarity reversal line on the photosphere below. The coronal helmet is an arcade-like structure on an even larger scale, straddling the polarity reversal line. Its fields are closed and rooted at two ends to the two sides of the photospheric polarity reversal line. The tunnel-like, low-density cavity at its base is identified with the prominence magnetic flux rope. The coronal helmet in Figure 17 has the fortuitous orientation of having its arcade length along the line of sight. This explains the visibility of the low-density cavity and the knotlike prominence seen along its length. Such a coronal helmet is kept in equilibrium with the following hydromagnetic features (Low & Hundhausen 1995). There is the confinement of the helmet

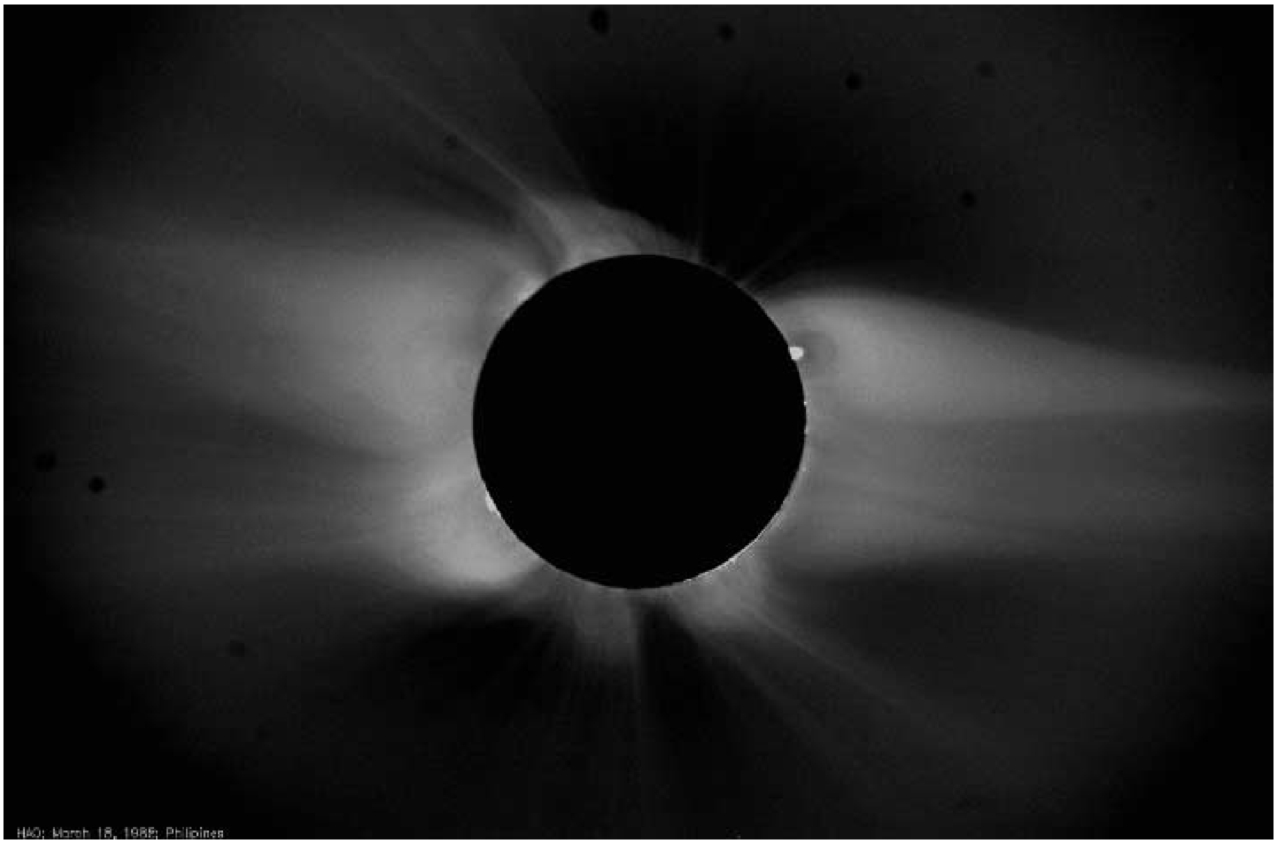

FIG. 17.—Total solar eclipse of 1988 March 18 showing a conspicuous three-part coronal helmet structure at the northwest limb as described in the text.

plasma by the external open fields on its two sides, along which the solar wind escapes. Inside the helmet, the cavity flux rope tends to expand out into interplanetary space but is confined by three agents: (1) the tension force of the closed, anchored helmet field; (2) the weight of the helmet plasma at coronal temperatures, and (3) the weight of the prominence at chromospheric temperatures.

5.2. *Hydromagnetic Structural Properties*

The flux-rope cavity is captured by the $\gamma_1 < 0$ solutions depicting an equatorial plasma depletion at the base of the $N = 6$ polytropic atmosphere. The small size of the cavity in Figure 17 suggests a tight packing of magnetic flux as modeled by a high-*n* twisted azimuthal flux rope (see Fig. 10). The $N = 6$ polytropic atmosphere is relatively cool with a negligible plasma pressure at large radial distances where the field dominates. In the real solar atmosphere, a thin boundary layer separates the plasma-dominated photosphere from the field-dominated low corona. This layer comprises the chromosphere, with a variable thickness of 10^3–10^4 km where the field is dominant, and a truly thin layer above it, only a few hundred kilometers thick. The latter, called the temperature transition region, is where the temperature rises steeply from about 10^5 K to the million degree temperature of the corona (Priest 1982; Zirin 1988). In our $\gamma_1 < 0$ solutions for the cool $N = 6$ atmosphere, the field-plasma interaction produces the large-scale field topology of a flux rope, but the simple stratification of the atmosphere belies the presence of such a field topology. Past modeling works usually take the lower boundary of the corona to be an infinitesimally thin boundary where field is anchored rigidly, as a first approximation. Our analysis suggests that a spatially resolved boundary layer may be important for our understanding of the magnetic structures on scales larger than the stratification scale height.

The "cool" $N = 6$, $\gamma_1 > 0$ solutions depict global density enhancement suggestive of the coronal helmet, but its temperature is unrealistically low so that at large radial distances, the field dominates. The "hot" $N = 11/3$ atmosphere is physically more realistic, with dominance of the plasma pressure at large radial distances. In either case, those $\gamma_1 > 0$ solutions describing a flux rope are too simple to represent the prominence and cavity realistically. For a more realistic morphological representation, we need to modify the simple polytropic plasma distribution given by equation (15) to more complex dependencies on the flux function A. The hot atmosphere of the $N = 11/3$ variety is to be retained on the global scale, while the cooler chromosphere-like boundary layer of the $N = 6$ variety dominates near the lower boundary to produce a low-density flux rope. In addition, an even cooler plasma enhancement must be introduced into the flux rope to represent the prominence mass.

The preceding survey of observations and theory shows that the prominence and coronal helmet may have roles to play in magnetic energy storage, as illustrated by our application of $E_{\rm CME}$ as an energy requirement. It should be emphasized that $E_{\rm CME}$ has been defined loosely by setting $\delta E = \Delta E$. The ratio of the energy excess δE above $E_{\rm Aly}$ to the free energy ΔE in the Aly open field varies with the circumstance of the equilibrium field. This ratio, being independent of the field amplitude B_0, describes an aspect of energy storage distinct from the total stored energy whose physical magnitude is fixed by B_0. The excess δE may be as small as 8% above $E_{\rm Aly}$, i.e., $\delta E \approx \frac{1}{5}\Delta E$, for a force-free field with a magnetic flux rope (e.g., Li & Hu 2003; Paper I), but is larger if that flux rope is confined via field-plasma interaction.

For the flux-rope force-free fields, a solar polar field of about 10 G, to fix B_0, can account for a total stored energy of the order of 2.3×10^{31} ergs, adequate for a CME-flare event. For the fast CMEs observed by Zhang et al. (2001, 2004), reconnection occurring early in the CME acceleration can liberate a part of ΔE associated with the Aly open field to drive the CME. Thus, energy additional to δE is also available for driving the CME. Fast CMEs typically originate from active regions where B_0 may be taken larger than used in our numerical estimates in § 4.2, in which case both δE and ΔE are significantly larger by their quadratic dependence on B_0. It has also been pointed out that force-free fields of complex, three-dimensional topologies may have energies significantly exceeding, by more than 8%, the limit $E_{\rm Aly}$ (Choe & Cheng 2002). These considerations show that force-free magnetic fields may store enough energy needed for CME-flare events. Field-plasma interaction is just an added degree of storing magnetic energy above those found in force-free fields. The presence of a prominence and coronal helmet prior to eruption, with masses of the order of 10^{15} g or larger in some significant events, suggests that this added degree of energy storage is important for this class of CMEs. The crucial element of a CME-producing magnetic structure, with or without field-plasma interaction, is the presence of a magnetic flux rope (Low 1994).

5.3. *Concluding Remarks*

Three-part coronal helmets and their almost daily eruptions into CMEs suggest that they are the natural products of solar activity (Gopalswamy et al. 2004; Low 2001; Low & Zhang 2005; Zhang & Low 2005). These helmets are as impressive in their propensity to erupt into CMEs as they are in their long-lived existence, days to weeks, prior to eruptions. As long-lived structures in the corona, they are built up over time to be energetically ready for spontaneous opening up of fields, CME expulsions, and flare heating associated with the reclosing of the opened field. There are two main aspects to understanding this hydromagnetic process, both presenting formidable nonlinear mathematical problems. The first is the challenge of understanding how the rich varieties of equilibrium states and their hydromagnetic stability and instability would naturally produce the three-part structures as the observed long-lived coronal structures. The other is the challenge of understanding the dynamics of CMEs as a time-dependent expulsion when sufficient magnetic energy has been stored in a coronal structure to break confinement. The study we have presented deals with the structural properties of idealized axisymmetric static atmospheres. Recently, Sun & Hu (2005) have taken the study of these properties of axisymmetric atmospheres to include the presence of the solar wind. These studies are steps toward answering the larger physical questions posed above.

We thank Gordon Petrie for comments and suggestions. The National Center for Atmospheric Research is sponsored by the National Science Foundation. This work is supported in part by the NASA Living with a Star Program and the NSF/ATM SHINE Program. B. F. acknowledges support by NSF grant DMS-0309803.

APPENDIX

$N = 3$ COOL POLYTROPIC ATMOSPHERE

We derive in closed form the global solution describing an $N = 3$ polytropic atmosphere embedding a dipolar poloidal ($B_\varphi = 0$) magnetic field. Take the pressure and density defined by the polytropic equation (7) to be of the form

$$p = a_0 A \left(\frac{r_0}{r} - \frac{r_0}{r_1}\right)^4, \tag{A1}$$

$$\rho = 4a_0 A \left(\frac{GM_\odot}{r_0}\right)^{-1} \left(\frac{r_0}{r} - \frac{r_0}{r_1}\right)^3, \tag{A2}$$

where a_0 is a free constant associated with the linear dependence of p and ρ on the magnetic flux function A. We have redefined r_1 to be a positive constant, with p and ρ vanishing at $r = r_1 > r_0$. This sets $r = r_1$ to be the top of the atmosphere at a cool polytropic temperature so that we may set p and ρ to be zero in the vacuum region $r > r_1$ where a magnetic field may exist. The spherical surface $r = r_1$ is therefore a free boundary across which the magnetic field $\boldsymbol{B}$ must be matched into a potential field in $r > r_1$. In order for $\boldsymbol{B}$ not to exert a discrete Maxwell stress on that boundary, $\boldsymbol{B}$ must be continuous across $r = r_1$ (Roberts 1967). Such free boundary problems are formidable in general, but an analytical solution can be constructed for our special case.

The problem we need to solve is posed by the field equations for a poloidal field:

$$\frac{\partial^2 A}{\partial r^2} + \frac{1-\mu^2}{r^2}\frac{\partial^2 A}{\partial \mu^2} + 4\pi a_0 r^2 (1-\mu^2)\left(\frac{r_0}{r} - \frac{r_0}{r_1}\right)^4 = 0, \qquad r < r_1, \tag{A3}$$

$$\frac{\partial^2 A}{\partial r^2} + \frac{1-\mu^2}{r^2}\frac{\partial^2 A}{\partial \mu^2} = 0, \qquad r > r_1, \tag{A4}$$

to be solved for A in $r > 1$ subject to the boundary conditions given by equation (14), supplemented by the boundary condition that both A and its derivatives are continuous across the free boundary $r = r_1$. In the units used in the paper that render $B_0 = r_0 = 1$, the desired solution is of the form

$$A = A_P + A_{\rm potential}, \tag{A5}$$

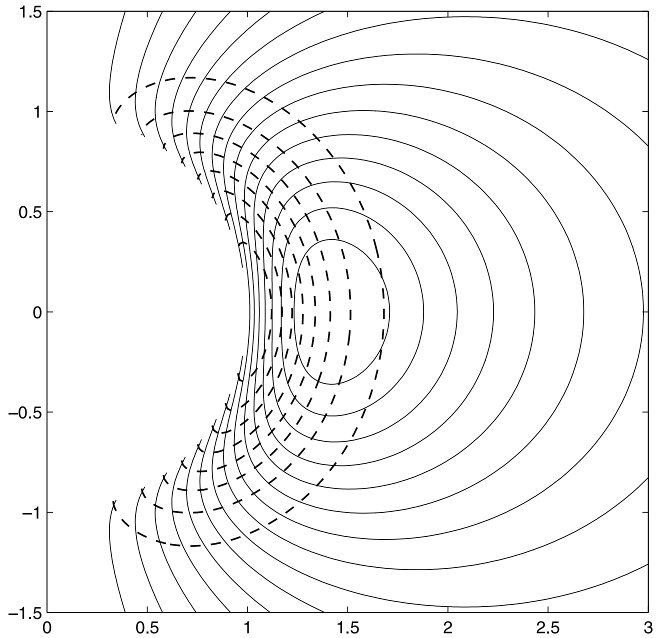

FIG. 18.—The $N = 3$ cool polytropic atmosphere with $a_0 = 1$, $r_0 = 1$, and a finite top at $r = r_1 = 3.0$ abutting vacuum in $r > r_1$ into which the atmospheric magnetic field lines (*solid lines*) extend smoothly as a vacuum potential field. The contours of constant density (*dashed lines*) indicate an enhancement associated with the closed fields located at the base of the atmosphere; the density is everywhere zero in $r > r_1$.

where $A_{\text{potential}}$ is a potential field defined for $r > 1$ and A_P is the particular solution to equation (A3) that is constructed to be zero everywhere in $r > r_1$ but takes the form

$$A_P = -\frac{2\pi a_0}{15 r_1^4} F(r) \sin^2\theta,$$

$$F = 60 r_1^2 r^2 \log\left(\frac{r}{r_1}\right) + 60 r_1 r^2 (r_1 - r) + 30 r^2 (r_1 - r)^2 + 20 r (r_1 - r)^3 - 5 (r_1 - r)^4 + \frac{2}{r}(r_1 - r)^5, \tag{A6}$$

in $r < r_1$. By this construction A_P and its derivatives vanish at $r = r_1$. It therefore follows that the solution given by equation (A5) and its derivatives are continuous everywhere in $r > 1$. Subject to the boundary conditions given by equation (14), we take $A_{\text{potential}}$ to be the potential dipole field

$$A_{\text{potential}} = \left(1 + \frac{2\pi a_0}{15 r_1^4} F|_{r=1}\right) \frac{\sin^2\theta}{r}. \tag{A7}$$

Substitution of A into equation (A1) gives the pressure and density distributions in $r < r_1$, keeping in mind that, by definition, p and ρ are zero in the vacuum region $r > r_1$. Figure 18 displays an illustrative solution. We leave the reader to explore these interesting solutions and return to the paper where we concentrate on static atmospheres that extend out to infinity.

REFERENCES

Allgower, E. L., & Georg, K. 1992, Acta Num., 1, 64
Aly, J. J. 1984, ApJ, 283, 349
———. 1991, ApJ, 375, L61
Amari, T., Luciani, J. F., Aly, J. J., Mikic, Z., & Linker, J. 2003a, ApJ, 585, 1073
———. 2003b, ApJ, 595, 1231
Amari, T., Luciani, J. F., Mikic, Z., & Linker, J. 2000, ApJ, 529, L49
Anzer, U., & Pneuman, G. W. 1982, Sol. Phys., 79, 129
Aschwanden, M. J. 2004, Physics of the Corona, An Introduction (New York: Springer)
Berger, M. A. 1984, Geophys. Astrophys. Fluid Dyn., 30, 79
Berger, M. A., & Field, G. B. 1984, J. Fluid Mech., 147, 133
Bommier, V. 1998, in ASP Conf. Ser. 150, New Perspectives on Solar Prominences, ed. D. Webb, B. Schmieder, & D. M. Rust (San Francisco: ASP), 4
Burkepile, J. T., Hundhausen, A. J., Stanger, A. L., St. Cyr, O. C., & Seiden, J. A. 2004, J. Geophys. Res., 109, A03103
Chandrasekhar, S. 1961, Hydrodynamic and Hydromagnetic Stability (Oxford: Oxford Univ. Press)
Chen, P. F., & Shibata, K. 2000, ApJ, 545, 524
Choe, G. S., & Cheng, C. Z. 2002, ApJ, 574, L179
Ciaravella, A., et al. 2000, ApJ, 529, 575
Courant, R., & Hilbert, D. 1963, Methods of Mathematical Physics, Vol. 2 (New York: Academic)
Cremades, H., & Bothmer, V. 2004, A&A, 422, 307
Dere, K. P., Brueckner, G. E., Howard, R. A., Michels, D. J., & Delaboudiniere, J. P. 1999, ApJ, 516, 465
Fan, Y. 2001, ApJ, 554, L111
Fan, Y., & Gibson, S. E. 2003, ApJ, 589, L105
———. 2004, ApJ, 609, 1123
Fan, Y., & Low, B. C. 2003, in ASP Conf. Ser. 286, Current Theoretical Models and Future High Resolution Solar Observations: Preparing for ATST, ed. A. A. Pevtsov & H. Uitenbroek (San Francisco: ASP), 347
Flyer, N., Fornberg, B., Thomas, S., & Low, B. C. 2004, ApJ, 606, 1210 (Paper I)
Fong, B., Low, B. C., & Fan, Y. 2002, ApJ, 571, 987
Fornberg, B. 1988, J. Fluid Mech., 190, 471
———. 1996, A Practical Guide to Pseudospectral Methods (Cambridge: Cambridge Univ. Press)
Gibson, S. E., Fan, Y., Mandrini, C., Fisher, G., & Demoulin, P. 2004, ApJ, 617, 600
Gibson, S. E., Foster, D. J., Guhatharkurta, M., Holzer, T. E., & St. Cyr, C. 2003, J. Geophys. Res., 108, SSH7-1

Gibson, S. E., & Low, B. C. 1998, ApJ, 493, 460
———. 2000, J. Geophys. Res., 105, 18187
Gilbert, H. R., Holzer, T. E., & MacQueen, R. M. 2005, ApJ, 618, 524
Gopalswamy, N., & Hanaoka, Y. 1998, ApJ, 498, L179
Gopalswamy, N., Yashiro, S., Vourlidas, A., Lara, A., Stenborg, G., Kaiser, M. L., & Howard, R. A. 2004, BAAS, 204, 4709
Heinemann, M., & Olbert, S. 1978, J. Geophys. Res., 83, 2457
Hiei, E., Hundhausen, A. J., & Sime, D. G. 1993, Geophys. Res. Lett., 20, 2785
Howard, R. A., Sheeley, N. R., Jr., Koomen, M. J., & Michels, D. J. 1985, J. Geophys. Res., 90, 8173
Howard, R. A., et al. 1997, Geophys. Monogr., 99, 17
Hu, Y. Q., Li, G. Q., & Xing, X. Y. 2003, J. Geophys. Res., 108, 1072
Hu, Y. Q., & Wang, Zh. 2005, ApJ, 623, 551
Hundhausen, A. J. 1977, in Coronal Holes and High Speed Solar Wind Streams, ed. J. B. Zirker (Boulder: Colorado Assoc. Univ. Press), 225
———. 1997, in Cosmic Winds and the Heliosphere, ed. J. R. Jokipii, C. P. Sonnett, & M. S. Giampapa (Tucson: Univ. Arizona Press), 259
———. 1999, in The Many Faces of the Sun, ed. K. Strong et al. (New York: Springer), 143
Hundhausen, J. R., Hundhausen, A. J., & Zweibel, E. G. 1981, J. Geophys. Res., 86, 11117
Hundhausen, J. R., & Low, B. C. 1994, ApJ, 429, 876
Illing, R. M. E., & Hundhausen, A. J. 1986, J. Geophys. Res., 91, 10951
Judge, P. G., et al. 2002, ApJ, 576, L157
Keller, H. K. 1987, Lecture on Numerical Methods in Bifurcation Problems (New York: Springer)
Klimchuk, J. 2001, in Space Weather, ed. P. Song & G. Siscoe (Washington, DC: AGU), 143–157
Kuhn, J. R., et al. 1999, ApJ, 521, 478
Leroy, J. L. 1989, in Dynamics and Structures of Quiescent Prominences, ed. E. R. Priest (Dordrecht: Kluwer), 77
Leroy, J. L., Bommier, V., & Sahal-Brechot, S. 1983, Sol. Phys., 83, 135
Li, G. Q., & Hu, Y. Q. 2003, Chinese J. Astron. Astrophys., 3, 555
Li, J., Raymond, J. C., Acton, L. W., Kohl, J. L., Romoli, M., Noci, G., & Naletto, G. 1998, ApJ, 506, 431
Lionello, R., Mikic, Z., Linker, J. A., & Amari, T. 2002, ApJ, 581, 718
Lipscy, S. 1998, Honors thesis, Univ. Colorado
Lites, B. W., & Low, B. C. 1997, Sol. Phys., 174, 91
Lites, B. W., Low, B. C., Martinez-Pillet, V., Seagrave, P., Skumanich, A., Frank, Z. A., Shine, R. A., & Tsuneta, S. 1995, ApJ, 446, 877
Lopez Ariste, A., & Casini, R. 2002, ApJ, 575, 529
Low, B. C. 1994, Phys. Plasmas, 1, 1684
———. 1996, Sol. Phys., 167, 217
———. 1999, in AIP Conf. Proc. 471, Solar Wind Nine, ed. S. R. Habbal et al. (New York: AIP), 109
———. 2001, J. Geophys. Res., 106, 25141
Low, B. C., Fong, B., & Fan, Y. 2003, ApJ, 594, 1060
Low, B. C., & Hundhausen, J. R. 1995, ApJ, 443, 818
Low, B. C., & Smith, D. F. 1993, ApJ, 410, 412
Low, B. C., & Zhang, M. 2002, ApJ, 564, L53
———. 2004, ApJ, 609, 1098
———. 2005, in Solar Variability and Its Effects on the Earth's Atmosphere and Climate, ed. J. Pap et al. (AGU Monogr. 122; Washington, DC: AGU), 51
Magara, T. 2004, ApJ, 605, 480
Manchester, W., IV, Gombosi, T., DeZeeuw, D., & Fan, Y. 2004, ApJ, 610, 588
Parker, E. N. 1963, Interplanetary Dynamical Processes (New York: Wiley)
Patsourakos, S., & Vial, J.-C. 2002, Sol. Phys., 208, 253
Pneuman, G. W., & Kopp, R. A. 1971, Sol. Phys., 18, 258
Priest, E. R. 1982, Solar Magnetohydrodynamics (Dordrecht: Reidel)
Roberts, P. H. 1967, An Introduction to Magnetohydrodynamics (New York: Elsevier)
Rusin, V., & Rybansky, M. 1982, Bull. Astron. Inst. Czechoslovakia, 33, 219
Rust, D. M. 1994, Geophys. Res. Lett., 21, 241
Sakurai, T. 1985, A&A, 152, 121
Schmahl, E., & Hildner, E. 1977, Sol. Phys., 55, 473
Sun, S. J., & Hu, Y. Q. 2005, J. Geophys. Res., 110, A05102
Tandberg-Hanssen, E. 1995, The Nature of Solar Prominences (Dordrecht: Kluwer)
Taylor, J. B. 1974, Phys. Rev. Lett., 33, 1139
Tripathi, D., Bothmer, V., & Cremades, H. 2004, A&A, 422, 337
Uchida, Y., & Low, B. C. 1981, J. Astrophys. Astron., 2, 405
Wolfson, R. 1993, ApJ, 419, 382
———. 2003, ApJ, 593, 1208
Wolfson, R., & Dlamini, B. 1997, ApJ, 483, 961
Zhang, J., Dere, K. P., Howard, R. A., Kundu, M., & White, S. M. 2001, ApJ, 559, 452
Zhang, J., Dere, K. P., Howard, R. A., & Vourlidas, A. 2004, ApJ, 604, 420
Zhang, M., & Low, B. C. 2001, ApJ, 561, 406
———. 2003, ApJ, 584, 479
———. 2004, ApJ, 600, 1043
———. 2005, ARA&A, in press
Zirin, H. 1988, Astrophysics of the Sun (New York: Cambridge Univ. Press)

AUTHOR QUERIES

Q1 Au: Your article has been edited for grammar, consistency, and to conform to ApJ journal style (see Instructions to Authors). To expedite publication, we generally do not query every routine grammatical and style change made to a manuscript, although all substantive changes have been noted. Please review the article carefully. Note that we may be unable to make changes that conflict with journal style, obscure meaning, or create grammatical or other problems. Also note that article proofs via PDF do not show corrections that will have been made by the typesetter's proofreader, which generally include corrections of errors of page layout, figure placement, and spacing and font mistakes; feel free to mark any errors you notice in these areas. Please also note that it is not ApJ style to have titles on figures. Any text appearing at the top of a figure, with the exception of an axis label, has been removed and incorporated into the legend. **When sending us your corrections, if you are writing them by hand, please print clearly. If sending a fax, please do not write too close to the margins of the page, as these are often cut off in fax transmission. Finally, please note that a delayed, incomplete, or illegible response may delay the publication of your article while we contact you.**